Bachelor Thesis

Investigation of strength of 3D-filament-printed metallic components

Nikhil Chandramohan Rane

Faculty of Technology and Bionics
Hochschule Rhein-Waal

Submitted in partial fulfilment of the requirements of the degree of

Bachelor of Science in Mechanical Engineering

First Supervisor:	Prof. Dr.-Ing. Peter Kisters
Second Supervisor:	Prof. Dr.-Ing. Stéphane Danjou
Date:	26 July, 2023

Thesis Title

Investigation of the strength of 3D-filament-printed metallic components

Author

Nikhil Chandramohan Rane
B.Sc. Mechanical Engineering
Matriculation Number : 22341
Summer Semester 2023

First Supervisor

Prof. Dr.-Ing. Peter Kisters
peter.kisters@hochschule-rhein-waal.de
Hochschule Rhein-Waal

Second Supervisor

Prof. Dr.-Ing. Stéphane Danjou
stephane.danjou@hochschule-rhein-waal.de
Hochschule Rhein-Waal

Place of Project

Hochschule Rhein-Waal
Marie-Curie-Straße 1
47533 Kleve

Dr. Sommer Werkstofftechnik GmbH
Hellenthalstraße 2
D-47661 Issum-Sevelen

Declaration of Authenticity

I hereby declare that this bachelor thesis titled "Investigation of the strength of 3D-filament-printed metallic components" was independently authored and crafted by myself to the best of my knowledge, and no help from third parties was used to produce this work. All contents and ideas drawn from external sources have been acknowledged and referred to in this thesis. The thesis has not been submitted to any other examining body. I agree that this document may be subject to electronic plagiarism check. For this purpose an anonymous copy may be distributed and uploaded to servers within and outside the Rhine-Waal University of Applied Sciences.

Nikhil Chandramohan Rane	Kleve , 25.07.2023
	Place, Date

Acknowledgement

First and foremost, I would like to thank Prof. Peter Kisters and Prof. Stéphane Danjou for supporting me throughout the thesis and answering all my questions with patience. Without their help and trust in me, this thesis would not have been possible. Moreover, I would also like to thank Martin Schlosser and Dr. Thomas Krenzel. They were always willing to assist and instruct me on how to operate the various machines that I needed to conduct my measurements.

I wish to extend my gratitude to Philipp Sommer for allowing me to use the facility of Dr. Sommer Werkstofftechnik GmbH for the metallographic analysis of the specimens.

Furthermore, I would like to thank my fellow students working with me in the Product Development Lab of Rhine-Waal University of Applied Sciences, especially the research assistant, Claudio Marzo. They always helped me and joined me for lunch. These breaks would often lead to interesting discussions about random topics, which I thoroughly enjoyed.

Lastly, I would like to thank my family and friends for their unending support and encouragement throughout the thesis process. Without their words of encouragement, I would not have been able to write my thesis with the same passion.

Abstract

Material Extrusion (MEX) 3D printing using metal-polymer filament is a new technology gaining popularity to make metallic 3D printed parts. The parts are printed similarly to MEX 3D printing using thermoplastic filament, with the extra steps of debinding and sintering. The technology has been explored and investigated to build up knowledge about it at Hochschule Rhein-Waal. The material strength of parts manufactured using this technology has been systematically investigated. Gaps in literature about surface roughness have been seen, and hence, the evolution of surface roughness from printed to sintered parts has been studied. The effect on the strength of material due to changes in surface roughness on surfaces parallel to the printing direction has also been experimentally studied. Lastly, primary metallographic analysis has been conducted on the printed and sintered samples.

As a result of the investigation, the strength of materials has been successfully determined, and the results obtained were found to be in agreement with a few studies in the literature. Furthermore, no change in strength has been observed with changes in surface roughness. It was also noticed that there was a clear increase in surface roughness after the debinding and sintering processes on the printed specimens. Moreover, metallographic analysis revealed a high level of porosity in the sintered specimens. MEX 3D printing using metal-polymer filament displayed vast potential during this study; however, further practical investigations are needed to study the applications of this technology.

Keywords

Additive Manufacturing; Material Extrusion; Tensile Strength; Surface Roughness; Metal-polymer Filament; Metallography; BASF Ultrafuse; Ultimaker

Contents

Declaration of Authenticity **ii**

Acknowledgement **iii**

Abstract **iv**

Contents **v**

List of Tables **ix**

List of Figures **xi**

Acronyms **xv**

1 Introduction **1**

1.1 Motivation 2

1.2 Objectives 2

1.3 Outline 3

2 State of the Art in Metal Material Extrusion 3D Printing **4**

2.1 Available 3D Printable Materials 5

2.2 Material Properties 6

2.2.1 Physical and Tensile Strength Properties 6
2.2.2 Surface Roughness 9
2.2.3 Metal MEX and MIM 10
2.2.4 Heat Treatment and Posorsity 10
2.3 Cost Modeling 11
2.4 BASF Metal Material Extrusion 3D Printing Recommendations . . . 12
2.4.1 Recommended Process Parameters 12
2.4.2 Recommended Design Guidelines 13
2.4.3 Shrinkage Plate 15

3 Technical Background 16

3.1 Material Extrusion 3D Printing 16
3.2 Metal Material Extrusion 3D Printing 17
3.2.1 Debinding 18
3.2.2 Sintering 18
3.3 Simulation 19
3.3.1 Debinding Simulation 19
3.3.2 Orientation Simulation 20
3.3.3 Sinter Simulation 21
3.4 BASF Metal-Polymer Material Filaments 21
3.4.1 Ultrafuse®316L 21
3.4.2 Ultrafuse®17-4PH 22
3.4.3 Ultrafuse®Support Layer 23
3.5 Post-Processing 23
3.6 Surface Roughness 24

3.6.1 Sa 24
3.6.2 Sz 25
3.6.3 Ssk 25
3.6.4 Sku 26

4 Experiments **27**
4.1 Equipment 27
4.1.1 Ultimaker S5 27
4.1.2 Tensile Test Machine 28
4.1.3 Surface Roughness Machine 29
4.2 Design of Experiments 29
4.2.1 Printing Orientations 29
4.2.2 Surface Roughness 30
4.2.3 Printing Material 30
4.2.4 Full Factorial Design of Experiments 30
4.3 Specimen Design 32
4.4 Execution Procedure 34
4.4.1 Shrinkage and Density 34
4.4.2 Tensile Test 35
4.4.3 Surface Roughness 36
4.4.4 Metallography 37
4.5 Specimen Fabrication 38
4.5.1 Initial Fabrications 38
4.5.2 Specimen Fabrication Trials 39
4.6 Limitations of Experiments 41

5 Data Evaluation and Discussion **43**

5.1 Visual Inspection 43

5.2 Shrinkage 44

5.3 Density 45

5.3.1 Green Parts 45

5.3.2 Sintered Parts 45

5.4 Surface Roughness 46

5.4.1 Unpolished Samples 47

5.4.2 Polished Samples 48

5.5 Tensile Test 50

5.5.1 17-4PH On-edge Unpolished Specimen 52

5.5.2 17-4PH Flat Unpolished Green Specimen 53

5.6 Chemical Composition 53

5.7 Metallography: Green State 54

5.8 Metallography: Unetched Sintered State 55

5.9 Metallography: Etched Sintered State 57

5.9.1 316L Samples 57

5.9.2 17-4PH Samples 62

5.10 Printing Complex Parts 64

6 Conclusion **66**

6.1 Potential of Metal Material Extrusion 3D Printing 67

7 Future Work **69**

A Appendix **i**

I Figures i

I.1 Surface Roughness ii

I.2 Metallography iv

I.2.1 Green Samples iv

I.2.2 Porosity Measurements v

I.2.3 Sintered Etched Samples vi

II Printing Parameters viii

List of Tables

2.1 Some commercially available metal-polymer filaments for MEX 3D printing. 5

2.2 Tensile test results [5]. 6

2.3 Comparison of tensile test results between manufacturer and as found by Tosto et al. [7]. 7

2.4 Porosity results of as-sintered, H900 and H1150 specimens [16]. . . . 11

2.5 Cost Modeling between Metal MEX 3D printed part and SLM printed part [7]. 12

2.6 Some recommended process parameters by BASF for metal MEX 3D printing [17]. 13

3.1 Brown part material property [25]. 20

3.2 Chemical Composition of sintered 316L part [14]. 22

3.3 Material Properties of sintered 316L part [14]. 22

3.4 Chemical Composition of sintered 17-4PH part [15]. 22

3.5 Material Properties of sintered 17-4PH part [15]. 23

4.1 Specifications of Ultimkaer S5 printer [35]. 28

4.2 Full Factorial Design of Experiments. 31

5.1 Density of 316L and 17-4PH parts in green state 45

5.2 Casted T-joint surface roughness parameters 47

5.3 Fracture strain [%] values of 316L and 17-4PH, along with released fracture strain values by BASF [14], [15]. The strain values are rounded off as per ISO 6892-1. 51

5.4 17-4PH on-edge unpolished specimen material properties. 52

5.5 17-4PH green part basic material properties. Ultrafuse PLA material properties extracted from [45]. 53

5.6 OES analysis results of sintered 316L part. 54

5.7 OES analysis results of sintered 17-4PH part. 54

5.8 EDX analysis results. Values measured in mass percentages. 59

A.1 Some important printing parameters used in Ultimaker S5 printer. . viii

List of Figures

1.1 3D printed metal bridge [1]. 1

2.1 Conventions used for build orientations [5]. 4

2.2 Model view of the specimens in the slicer. a) build orientations of 17-4PH specimens b) Infill percentage of ZX (upright) specimen c) Infill percentage of XY (flat) specimen [7]. 7

2.3 Tensile test results showing influence of layer height and build orientation on tensile strength [8]. 8

2.4 Tensile test results showing influence of flow rate on tensile strength of 17-4PH green parts [11]. 9

2.5 Metal MEX 3D printer and SLM printer surface roughness results in the study [5]. 10

2.6 Temperature profile of H900 and H1150 processes [16]. 11

2.7 Recommended height-to-width ratio [17]. 14

2.8 Green part with shrinkage plate [22]. 15

2.9 Warped shrinkage plate [22]. 15

3.1 Metal Material Extrusion 3D printing process or metal FFF printing as per Ultimaker [17]. 17

3.2 Pictorial example of Sa [32]. 25

3.3 Pictorial example of Sz. Sp represents highest peak and Sv represent deepest pit [32]. 25

3.4 Pictorial example of Ssk [32]. 26

3.5 Pictorial example of Sku [32]. 26

4.1 Ultimaker S5 [36]. The red box indicates the Air Manager. 28

4.2 Layered sample in green state. 31

4.3 E5x16x50 form specimen according to DIN 50125 32

4.4 E4x10x35 form specimen according to DIN 50125 33

4.5 Specimens in the green state. 34

4.6 Stroke rate used in tensile testing. 36

4.7 Nanovea PS50 profilometer workbench with a vice holding a specimen. 36

4.8 Points depicting the centers of areas selected for surface roughness measurements 37

4.9 Metal and PLA rings. The metal ring is slightly polished. 39

4.10 Cracked on-edge tensile bar. This is the first iteration. 40

4.11 On-edge warped tensile bar after changing printing parameters as per [22]. 40

4.12 Cracked on-edge tensile bar on sintered support. This is the second iteration. 41

5.1 Shrinkage bar graph. Error bars represent the maximum and minimum values in the sample space. 44

5.2 Density bar graph. Error bars represent the maximum and minimum values in the sample space. 46

5.3 Casted T-joint 46

5.4 Surface roughness evolution in unpolished 316L specimens with the D&S process. Error bars represent the maximum and minimum values in the sample space 47

5.5 Surface roughness evolution in polished 316L specimens with the D&S process. Error bars represent the maximum and minimum values in the sample space 49

5.6 Kurtosis areal roughness parameter of 17-4PH specimens. Error bars represent the maximum and minimum values in the sample space . . 49

5.7 Strength properties of 316L and 17-4PH materials. 50

5.8 Tensile tested specimens showing necking. 52

5.9 25x zoom micrographs of green state of crosswise samples 55

5.10 25x Zoom micrographs of unetched sintered samples 56

5.11 100x zoom micrograph of 316L crosswise unetched sintered sample. . 57

5.12 100x and 500x zoom micrographs of 316L lenghtwise etched samples 58

5.13 EDX analysis positions 59

5.14 Phase diagraom of 316L [46] 60

5.15 316L Murakami etched sample 61

5.16 316L microstructure [48] 61

5.17 100X and 500X Zoom micrographs of 17-4PH lenghwise sintered state of the samples 62

5.18 17-4PH phase diagram [46] 63

5.19 MIM 17-4PH microstructure sintered in PADS furnance [50]. 63

5.20 M10 screw in a 3D printed threaded hole. 64

5.21 Cracked turbine blade after D&S process. 64

5.22 Miniature model of turbine blade printed using Metal MEX technology 65

5.23 Sintered layered sample consisting of two separate layers: 316L and 17-4PH 65

A.1 Rough surface of the specimen that was milled afterwards. i

A.2 Different shrinkages in the length of 17-4PH and 316L specimens. . i

A.3 Plot of surface rouhness parameters of 17-4PH unpolished specimens. ii

A.4 Plots of surface rouhness parameters of 17-4PH polished specimens. iii

A.5 25x zoom micrographs of green lengthwise samples. iv

A.6 Porosity measurements in unetched sintered samples. v

A.7 Micrographs of 316L sintered crosswise etched samples. Etched with V2A solution. vi

A.8 Micrographs of 17-4PH sintered crosswise etched samples. Etched with V2A solution. vii

A.9 100x zoom micrographs of 316L sintered crosswise etched samples. Etched with Murakami reagent. vii

Acronyms

ρ_{theo}	Theoretical Density
ρ_{wd}	Density
ε	Elongation at Break
17-4PH	BASF Forward AM Ultrafuse®17-4 PH filament
316L	BASF Forward AM Ultrafuse®316L filament
ADAM	Atomic Diffusion Additive Manufacturing
AM	Additive Manufacturing
BASF	BASF Forward AM
BDM	Bound Metal Deposition
D&S	Debinding and Sintering
DMLS	Direct Metal Laser Sintering
DOE	Design of Experiments
EBM	Electron Beam Melting
EDX	Energy-dispersive X-ray Spectroscopy
FDM	Fused Deposition Modeling

FDMet	Fused Deposition of Metals
FFF	Fused Filament Fabrication
LOM	Light Optical Metallography
MEX	Material Extrusion
MIM	Metal Injection Moulding
OES	Optical Emission Spectroscopy
POM	Polyoxymethylene
Rm	Tensile Strength
Rp0.2	Yield Strength
S5	Ultimaker S5
SEM	Scanning Electron Microscope
SLM	Selective Laser Melting
SS	Stainless Steel
support material	BASF Forward AM Ultrafuse®Support Layer
WAAM	Wire and Arc Additive Manufacturing
XRD	X-Ray Diffraction

Chapter 1

Introduction

In the media, Additive Manufacturing (AM) is always portrayed as a part of technologically advanced society. With the advent of AM during the 1990s and early 2000s, endless possibilities opened up for prototyping and manufacturing. Initially, AM was mainly found in industry and research contexts, where it was used to produce thermoplastic and metal-powder parts using technologies such as fused deposition modeling and selective laser melting. However, with expiring patents, AM became widely available, and many cheap and easily accessible printers started entering the market. This led to an increase in attention from the media and the general public towards AM technologies. From thermoplastic 3D printing to, more recently, metal 3D printing, the technology has grown leaps and bounds. One famous example of metal 3D printing is the MX3D bridge in Amsterdam, as seen in Figure 1.1, printed using Wire and Arc Additive Manufacturing (WAAM).

Figure 1.1: 3D printed metal bridge [1].

An example of metal 3D printing technology that has been recently developed uses commercially available Material Extrusion (MEX) 3D printers with metal-polymer filament to print metal-polymer parts. These parts need to undergo Debinding and Sintering (D&S) process to become final metal parts[2]. In this thesis, this particular technology has been explored.

1.1 Motivation

The technology to produce metal parts using metal-polymer filament inhouse opens the door to easy design of strong and customizable industry ready parts. Previously, the MEX 3D printed parts were only used for prototyping, especially in industry, due to their low strength. However, with metal MEX 3D printing technology, this could soon change. Also, this technology has huge economic potential as it could be used with many commercially available hobby grade MEX 3D printers. Thus, increasing the accessibility of metal part printing to the masses as the printing could be done inhouse and the D&S process could be outsourced. Other metal 3D printing technologies, such as Selective Laser Melting (SLM), Electron Beam Melting (EBM), Direct Metal Laser Sintering (DMLS), etc, have high investment costs because of specific printing conditions such as vacuum, high energy lasers, etc. For example, the approximate cost of a mid-range SLM printer is around $1 million[3]. This costs many folds more compared to MEX 3D printers. Therefore, the economic aspect of this technology also makes it intriguing to investigate.

Motivated by these reasons, this document aims at exploring the new metal MEX 3D printing technology specifically, studying the strength of the MEX 3D printed material and how it changes with modifications in some parameters such as surface roughness and build orientation.

1.2 Objectives

One of the primary objectives of this thesis is to build knowledge within Hochschule Rhein-Waal on how to make metal parts using metal MEX 3D printing. Moreover, the strength of metal MEX 3D printed parts is chosen as a material property of interest to be explored. Also, there seems to be a gap in the literature regarding the effect of changes in surface roughness on the strength of materials. This document will experimentally investigate this via a comparison between polished and unpolished (as-printed) specimens. It is observed that the surface of the specimens, parallel to the printing direction (layer side), has layer marks, which results in surfaces with a high surface roughness. It is hypothesized that by decreasing this high surface roughness, the tensile strength of the material will increase. In addition to

this, another objective is to fabricate tensile test bars with different build orientations and test how this affects the strength of the metal MEX 3D printed material. Finally, primary metallographic analysis is also planned to get the chemical composition and microstructure of the materials used for printing.

To achieve the above planned objectives, an Ultimaker S5 with a metal expansion kit was used. BASF Forward AM provides two certified metal-polymer filaments - Ultafuse 316L and 17-4PH. These materials are used because they are readily commercially available and Ultimaker certified. Furthermore, to procure strength data, tensile testing was performed. The surface roughness data was collected using an optical profilometer, and additionally, physical properties such as density and shrinkage values in the parts were also noted. In addition, Dr. Sommer Werkstofftechnik GmbH in Issum, Germany, was contacted to conduct metallographic analysis at their esteemed facility.

Keeping the above stated objectives in mind, the thesis is expected to accumulate experimental data about the material properties of the two materials used. These properties are compared with the manufacturer's released data and literature data to draw conclusions. Also, as a result of this study, it is expected to fill a literature gap concerning the effect that a change in surface roughness could have on the strength of the materials used. Further, metallographic analysis is expected to give insight on the microstructure and chemical composition of the materials, which could help in the determination of possible future post-processing treatments to acquire desired material properties.

1.3 Outline

This document is divided into seven chapters. After describing the thesis topic and motivation in Chapter 1, Chapter 2 deals with reviewing existing literature. Chapter 3 describes the technical background knowledge needed to understand the thesis. In the subsequent chapter, the methodology of the experiments and the limitations of the experiments are stated. Chapter 5 presents the experimentally collected data in a visually easy-to-understand way and discusses the results. Chapter 6 concludes the thesis, followed by Chapter 7, which has suggestions for future work.

Chapter 2

State of the Art in Metal Material Extrusion 3D Printing

In literature, it is often seen that many naming conventions are used to describe similar technologies. For this reason, a naming convention from international standards ISO/ASTM 52900 is followed so that this thesis can be comprehensible to a wider range of audiences. The technology commonly referred to as Fused Filament Fabrication (FFF) or Fused Deposition Modeling (FDM) comes under the umbrella term Material Extrusion (MEX) [4]. In this study, MEX 3D printing using metal-polymer filament is referred to as metal MEX 3D printing.

Conventions for build orientations of 3D printed specimens used in this thesis are as per the Figure 2.1 below:

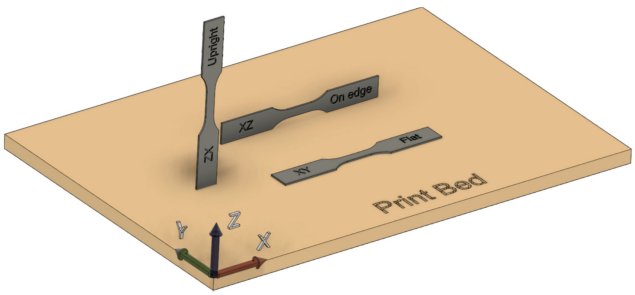

Figure 2.1: Conventions used for build orientations [5].

In this chapter, the studies and research conducted on metal MEX 3D printing will be explained. It is important to take note that this research in no way encompasses the entire research present, and there might be more literature present. This section is essential to understand the existing research done on the topic in relation

to mechanical properties and surface roughness in metal MEX 3D printing. In addition, by comparing the known literature results to the thesis results- similarities, distinctions, and potential areas of agreement or disagreement between the results and those in the literature can be identified.

Metal MEX 3D printing systems have gained plenty of attention in recent years due to their promise. Several manufacturers have researched and released metal MEX 3D printers in the late 2010s, with printers capable of printing at high temperatures and accurate material deposition so that structural integrity could be maintained. Different printers come with different build volumes, extrusion capabilities, software, and bed leveling capabilities. The user could choose a printer suited for their use case, considering part size, material composition, and precision.

2.1 Available 3D Printable Materials

One of the most important components in metal MEX 3D printing is the metal-polymer filament, which is melted and deposited layer by layer to form the raw part. This part is called the green part. Usually, metal powder is mixed with a polymer binder so that printability and structural integrity can be maintained. Many different materials are commercially available on the market. This gives the user flexibility to pick the appropriate material to achieve the desired metal final product [6]. Some of the metal-polymer filaments are listed in Table 2.1.

Table 2.1: Some commercially available metal-polymer filaments for MEX 3D printing.

Serial No.	**Metal Material**	**Manufacturer**
1	316L Stainless Steel, DIN 1.4404	BASF Forward AM
2	17-4 PH Stainless Steel, DIN 1.454	BASF Forward AM
3	A2 Tool Steel, DIN 1.2363	Makforged, Desktop Metal
4	D2 Tool Steel, DIN 1.2379	Makforged, Desktop Metal
5	H13 Tool Steel, DIN 1.2344	Makforged, Desktop Metal
6	Inconel 625	Makforged, Desktop Metal
7	Copper	Makforged, Desktop Metal
8	Aluminium 6061	Desktop Metal
9	Titanium 64-5	Desktop Metal
10	Tungsten	Desktop Metal

2.2 Material Properties

In current literature, the mechanical properties of 316L grade Stainless Steel (SS) printed via MEX have been studied more intensively than those of other materials, such as 17-4 PH grade SS. Many studies have been conducted that analyse how tensile strength is affected by changes in parameters such as layer height and build orientation. These studies provide an important starting point for a basic understanding of the impact of different 3D printing parameters on the strength of materials.

2.2.1 Physical and Tensile Strength Properties

A recent research [5] indicates that metal MEX specimens' tensile strength is significantly lower than that of specimens made using selective laser melting (SLM). This discrepancy is attributed to the rough surface, and porosity in the metal MEX manufactured specimens. All the specimens were printed in ZX orientation. The specimens printed using SLM technology were from the EOS M290 SLM printer and the Renishaw AM 400 printer. The EOS M290 specimens were heat treated at 700°C for 2 hours to relieve stress. Some of the results found by Kedziora et al. [5] are given in the Table 2.2:

Table 2.2: Tensile test results [5].

Parameters	Markforged 17-4 PH	BASF Ultrafuse 316L	EOS M 290 316L (HT)	Renishaw AM 400 316L
Yield strength, R_e, MPa	441.0 ± 55.4	152.9 ± 61.3	375.2 ± 22.4	443.1 ± 15.7
Tensile strength, R_m, MPa	495.9 ± 77.0	314.0 ± 41.7	533.2 ± 1.1	570.8 ± 4.4
Elongation at break A, %	0.4 ± 0.1	10.2 ± 5.0	38.2 ± 0.1	38.4 ± 0.1
Young's modulus, E, GPa	142 ± 65	160 ± 22	190 ± 18	129 ± 17

Furthermore, a similar research [7] showed that the results achieved were not comparable to mechanical properties published by the manufacturer (refer Table 2.3). However, it is stated that this could be because of the several defects, such as pores, inclusions, and poor interlayer bonding, found in the specimens and also the fact that the infill was not 100% as seen in refer Figure 2.2. The infill percentage was approximately 58% and 90% for 17-4 PH and 316L, respectively. It was concluded that the porosity seen in the specimens could act as a stress amplifier, causing early failures.

Some interesting points made by Tosto et al. [7] were that the internal structure of BASF 316L filament material showed metal particles from 1μm to 10μm in diameter embedded in polymeric strands. Additionally, the green parts printed using 316L with 100% infill had some voids, possibly due to unfinished fusion between layers

Table 2.3: Comparison of tensile test results between manufacturer and as found by Tosto et al. [7].

Material	Building Orientation	Yield Strength MPa	Tensile Strength MPa	Tensile Modulus GPa	Strain at Break %
316L	Flatwise	148.01 ± 4.50	443.90 ± 5.87	157.24 ± 4.50	43.33 ± 2.53
	Upright	113.75 ± 13.42	206.27 ± 80.11	117.31 ± 1.94	13.35 ± 6.59
17-4 PH	Flatwise	443.00 ± 6.90	497.40 ± 9.90	108.00 ± 6.90	0.79 ± 0.05
	Upright	412.00 ± 31.60	494.70 ± 29.70	102.8 ± 1.20	0.95 ± 0.14
316L *	Flatwise	251	561	–	53
	Upright	234	521	–	36
17-4 PH *	Flatwise	1100	1250	170	6
17-4 PH **	-	660	1042	195	8.5

* The data were extracted from the technical data sheet (TDS) released by the producer (BASF for the 316L and Markforged for the 17-4 PH).
** The data were extracted from the technical data sheet released by Desktop Metal with their Studio System™.

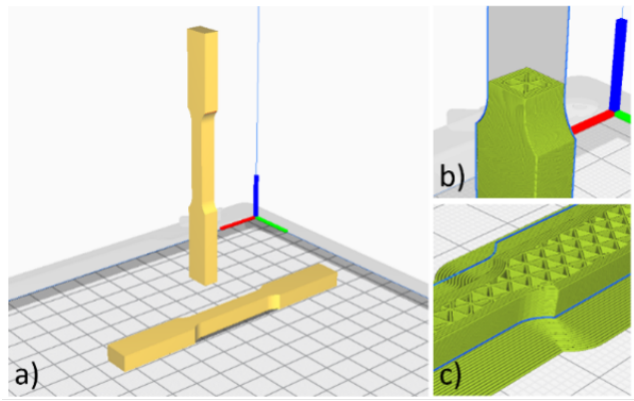

Figure 2.2: Model view of the specimens in the slicer. a) build orientations of 17-4PH specimens b) Infill percentage of ZX (upright) specimen c) Infill percentage of XY (flat) specimen [7].

.

during printing. After sintering, shrinkage of 20% in the XY plane and 25% in the printing direction (Z-axis) was also observed.

In another study [8], the impact of printing direction on the physical mechanical properties such as relative density, dimensional linear shrinkage, and tensile strength were examined. The paper uses three orientations : T, which represents XY orientation; W, which represents XZ orientation; and L, which represents ZX orientation. Additionally, two different layer heights were also used: 0.1mm and 0.3mm. A 316L Stainless Steel (SS) filament was used with 60% vol. 316L SS particles and 40% organic binder provided by Taisei Kogyo Co. Ltd. (Osaka, Japan). Interestingly, in this paper Debinding and Sintering (D&S) process was performed in the same vacuum furnace. Thermal debinding was used to debind the green parts (600°C for 2 hours) and sintering was consecutively performed at 1280°C for further 2 hours.

Regarding the tensile strength of 316L in the above mentioned study, the specimens printed with the XY orientation gave the highest ultimate tensile strength and strain results, followed by the XZ orientation. The results from the ZX orientation were seen to be significantly lower than the other two orientations (see Figure 2.3). Moreover, specimens printed with a lower layer height showed greater ultimate tensile strength and strain at break.

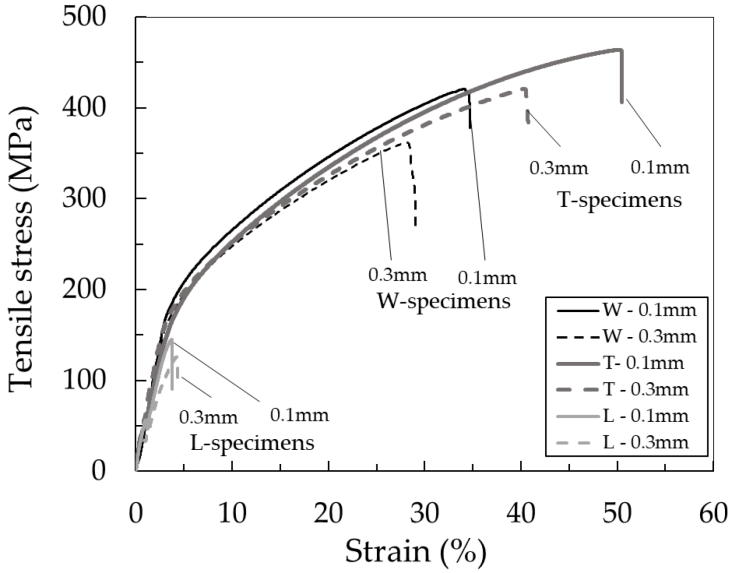

Figure 2.3: Tensile test results showing influence of layer height and build orientation on tensile strength [8].

Lastly, the paper concludes that the relative density is approximately the same irrespective of the layer direction, but with a change in layer height, the relative density changes. The relative density is higher with lower layer heights. In addition, all the green parts faced anisotropic shrinkage, with maximum shrinkage in the layer printing direction. The shrinkage was 15–17% in the layer printing direction (Z) and 14–15% in the perpendicular direction of layer printing (X,Y).

A further research from Tosto et al. [9] studies the connection between tensile strength and 3 parameters - flow rate, nozzle temperature, and layer height. BASF 316L filament was used and it was observed that flow was the most important factor which affected the tensile strength. It was concluded that more flow rate leads to improved sample density and less porosity. It was also observed that an increase in layer height from 90 micrometer to 140 micrometer leads to better tensile strength as there are less discrepancies due to fewer printed layers. This result is not in agreement with the results obtained in the previously mentioned paper [8], where an inverse relation between tensile strength and layer height was observed.

Metal MEX 3D printing of 17-4PH has not been widely studied in the literature in terms of 3D metal filament printing. In the research paper [10], the mechanical properties of the 17-4 PH filament are studied with a filament 55 vol% of 17-4PH SS. It was found that the average Young's modulus was 196 GPa, the average tensile strength was 696 MPa and the fracture strain was 4%. In another paper [11], the connection between flow rate and tensile strength of green parts was shown. In the paper, the flow rate was increased from 95% to 127% and with an increase of flow rate, there was a clear increase in tensile strength as shown in Figure 2.4.

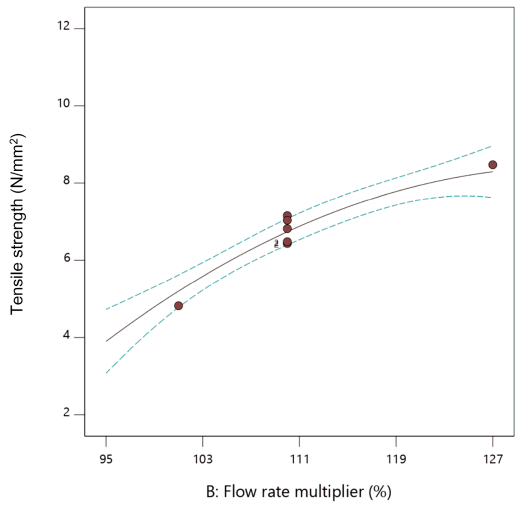

Figure 2.4: Tensile test results showing influence of flow rate on tensile strength of 17-4PH green parts [11].

2.2.2 Surface Roughness

A previously mentioned study [5] also presented surface roughness results along with tensile strength results. It compared the surface roughness of metal MEX 3D printing and SLM. For metal MEX 3D printing, BASF 316L and Markforged 17-4PH metal-polymer filaments were used. For SLM, EOS M290 and the Renishaw AM 400 SLM printers were used to print 316L SS. The specimens printed using EOS M290 were stress relief heat treated at 700°C for 2 hours. The results found in this study are presented in the Figure 2.5. The metal MEX printers in the study showed more surface roughness than SLM printed parts.

Surprisingly no other study have been found with results regarding surface roughness. This may be due to the fact that the technology was only introduced within the last few years.

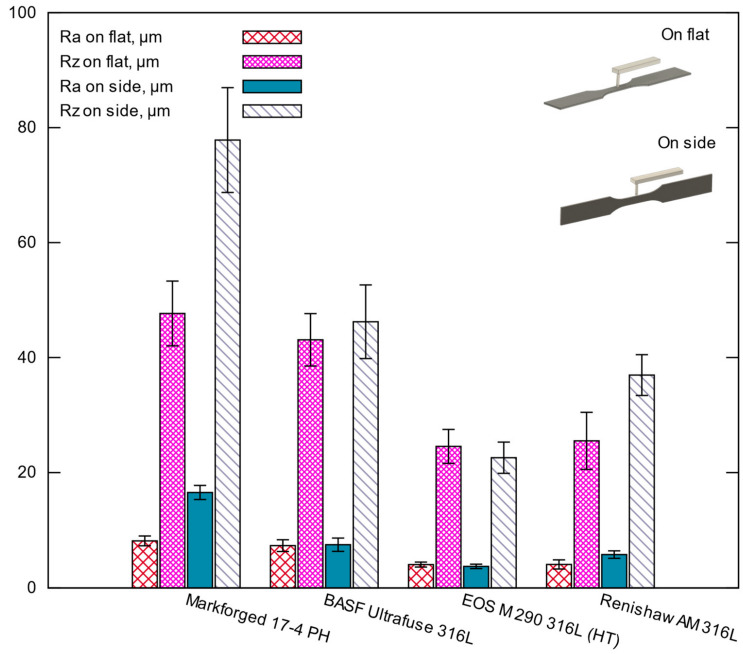

Figure 2.5: Metal MEX 3D printer and SLM printer surface roughness results in the study [5].

2.2.3 Metal MEX and MIM

The properties of metal MEX and Metal Injection Moulding (MIM) are also of interest, as both processes go through the same debinding and sintering processes. The difference is in the creation of the green part. For MIM, the melted metal-polymer feedstock is injected into the mold [12], whereas in MEX, the green part is made by placing layer upon layer of melted metal-polymer filament to achieve the desired shape. A research [13] have extensively compared the two technologies and concluded that the mechanical properties of metal MEX 3D printed parts, such as tensile strength and elongation, are comparable to those of MIM parts. These results are also in accordance with those released by BASF for their 316L and 17-4PH filaments [14], [15].

2.2.4 Heat Treatment and Posorsity

One recent study [16] investigated the impact of heat treatment on porosity of 17-4PH MEX 3D printed parts. Three MEX technologies were analysed: FFF, Atomic Diffusion Additive Manufacturing (ADAM), and Bound Metal Deposition (BDM). These three technologies are very similar to metal MEX 3D printing, and

thus research results in these areas could be studied. ADAM technology has been trademarked by Markforged Inc. and BDM technology has been trademarked by Desktop Metal Inc. The material used for printing was 17-4PH SS. For FFF printing, BASF 17-4PH filament was used. The paper concluded that porosity was decreased and hardness was increased after H900 heat treatment. Moreover, after H1150 heat treatment, the porosity and hardness both decreased (refer Table 2.4 for porosity results). The ADAM and FFF technologies are more susceptible to heat treatment in terms of change in porosity and hardness. One common result of both H900 and H1150 heat treatments is decrease in porosity compared to the as-sintered specimens [16]. The decrease in porosity as shown in the paper, could also directly result in better strength properties of material. However, further analysis is needed to confirm this. The temperature profile of the heat treated specimens are shown in Figure 2.6.

Table 2.4: Porosity results of as-sintered, H900 and H1150 specimens [16].

	Porosity (%)		
Technology	As-sintered	H900	H1150
ADAM	2.4	2.0 (−18.4%)	1.6 (−32.2%)
BMD	1.8	1.6 (−10.8%)	1.8 (−1.5%)
FFF	2.2	1.5 (−34.3%)	1.8 (−21.3%)

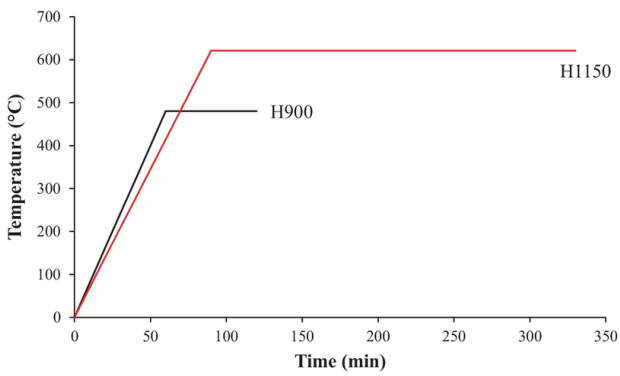

Figure 2.6: Temperature profile of H900 and H1150 processes [16].

2.3 Cost Modeling

The study [7] also presents cost modeling between 316L printed using MEX and SLM technologies by printing mould designs. The results are stated in Table 2.5. It is important to note, though, that the part referred to in the table is the green part, and further sintering costs need to be added. Nonetheless, it can be seen that the

cost of SLM technology is considerably higher than the cost of parts produced using MEX technology. This shows the potential of producing metal parts using MEX technology.

Table 2.5: Cost Modeling between Metal MEX 3D printed part and SLM printed part [7].

	Ultrafuse 316L		**SLM 316L**	
	%	**EUR**	**%**	**EUR**
Material	40.9	100.62	28.8	330.13
Build prep	28.4	70.00	18.3	210.00
Machine usage	0.5	1.25	37.3	428.47
Build consumables	0.2	0.58	5.1	59.02
Labor	23.8	58.68	6.6	75.26
Post-process	6.1	15.00	3.9	45.00
Total cost		**246.13**		**1147.88**

2.4 BASF Metal Material Extrusion 3D Printing Recommendations

In this study, an Ultimaker S5 equipped with a metal expansion kit provided by Ultimaker in collaboration with BASF Forward AM (BASF) was used to print the green parts. Considering this new technology of metal MEX printing, BASF has given its users lots of recommendations so that any newcomers to the field could have a smooth entry into the technology. They have used their experience and listed out a few printing parameters and design guidelines for the users to follow for a successful printing and D&S process. The following subsections describe the recommendations.

2.4.1 Recommended Process Parameters

In order to get successful metal prints, BASF gives a few printing parameters for the slicing software. From their experience, BASF found these parameters to be the most efficient in printing a successful part. These parameters are given in the Table 2.6. It is also recommended to turn off the fan cooling so that the possibility of warpage can be reduced.

Table 2.6: Some recommended process parameters by BASF for metal MEX 3D printing [17].

Parameter	**Recommendation**
Extrusion multiplier	Single Wall Calibration
Retraction distance (direct/bowden)	1.5 mm / 5 mm
Retraction speed	45 mm/s
Layer height	0.1 - 0.25 mm
Infill Density	105%
Outline overlap percentage	20 - 35%, can also go higher
Nozzle temperature	230 - 250° C
Bed temperature	90 - 105° C
Print speed	25 mm/s
X and Y oversizing factors	120%
Z oversizing factor	126%

2.4.2 Recommended Design Guidelines

BASF has given a few design guidelines for the users to follow so that they could get a successful green part and, more importantly, so that the green part will successfully survive the D&S process. This is the part of the process where the printed part is most vulnerable. Usually, the printed green parts look very stable, but many times it may happen that during the D&S process the part collapses or gets deformed. To prevent this, BASF has provided 11 design guidelines that could be followed for successful finished metal parts. The guidelines [17] are described briefly below:

1. The print should fit in a volume of 100 x 100 x 100 mm. Additionally, BASF recommends, for best results, a green part volume of 60 x 60 x 60 mm. The prints bigger than 100 x 100 x 100 mm have a higher probability of failure. Moreover, permission from BASF, the developer of the metal-polymer filaments, has to be obtained in case the D&S process is to be done at a partner facility.

2. A height-to-width ratio of 3:1 should be maintained for the whole green part as shown in Figure 2.7.

3. The parts shrink the most in the printing Z direction. This is regardless of the orientation the green part is kept in for D&S process. It is recommended to have identical printing and D&S orientations.

4. Overhang angles greater than 45 degrees require support.

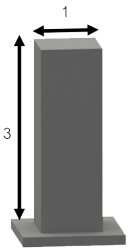

Figure 2.7: Recommended height-to-width ratio [17].

5. The walls that are not supported should maintain a 1:6 width-to-height ratio to prevent collapse of the wall.

6. Thin features in the part should be a whole number multiple of the nozzle diameter used. In case of this thesis, the nozzle diameter is 0.4 mm. Hence, the thin features should be at least 0.8 mm.

7. The green parts will shrink dramatically after the D&S process. Therefore, the green part should be scaled up during printing to compensate for the shrinkage faced afterwards.

8. Green parts with non-flat bottom surfaces are prone to tilting, warping, and collapse during the D&S process due to the presence of gravity, which means that the part will deform because of its own weight.

9. Horizontal holes larger than 8 mm could be printed with supports so that the shape is maintained. Smaller than 8 mm don't need support, but if needed, supports could be printed for safety. Larger holes could be modified to have a raindrop shape to compensate for distortion or collapse.

10. Vertical holes greater than 1.5 mm in diameter have a higher probability of success.

11. If two surfaces are very close to each other, then a gap of at least 0.75 mm should be maintained to prevent co-sintering of the surfaces.

In addition to the above guidelines, it is recommended to use a shrinkage plate to prevent distortion in the part. More information is provided in subsection 2.4.3. Some other manufacturers such as Markforged Inc. and Desktop Metal Inc. also have there own design guidelines for printing metal parts using their own trademarked technologies. These technologies are similar to the technology used by Ultimaker and BASF. Hence, exploring there guidelines could also prove to be informative as these documents have information on printing threads, and post-processing of final metal parts. For more information refer [18], [19].

2.4.3 Shrinkage Plate

It is recommended to print the part on a raft. This raft is called a "shrinkage plate". This plate provides a base for the part, and the top layers of this raft are covered with the support material consisting of Polyoxymethylene (POM). POM has good sliding characteristics, and this helps the part to comfortably shrink [20], [21]. The white layer in the Figure 2.8 represents the support layer, and below that is the shrinkage plate, which comes off after the D&S process.

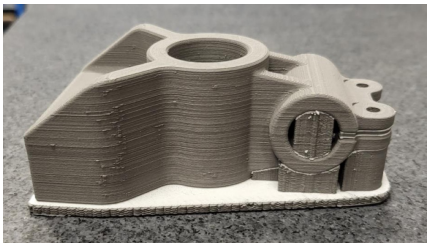

Figure 2.8: Green part with shrinkage plate [22].

BASF also recommends having a thick raft; possibly the middle layers should be more than 10. This ensures that a thick enough raft is printed so that post processing on the raft is possible. Sometimes the raft could be warped, especially if the part is very long. The bottom of the raft could be planarized using sand paper, a milling machine, or a grinder. It is very critical to have a planarized bottom, as after the debinding step, most of the binder is removed, which leads to the part losing most of its structural stability. Furthermore, gravity could induce critical stress if the bottom surface is not planar, which might lead to cracks. According to BASF, even a gap of around 0.15mm between the sides and center of the raft could cause a crack in the part (refer Figure 2.9). One simple way to check if the shrinkage plate is warped is by trying to put pressure by finger on one corner of the shrinkage plate. If the opposite corner lifts up, it is then an indication of a warped shrinkage plate [22].

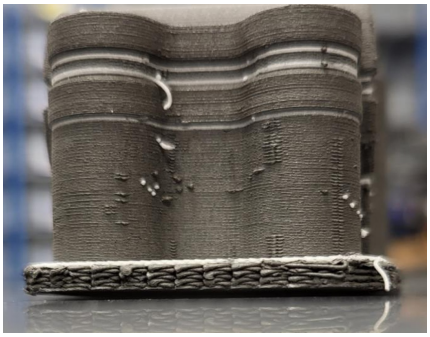

Figure 2.9: Warped shrinkage plate [22].

Chapter 3

Technical Background

This chapter describes the technical knowledge needed to understand the thesis. The section starts by describing the technology of MEX 3D printing used in the Ultimaker S5 3D printer, followed by its unique application to printing metallic material. Ultimaker states that it uses FFF technology, which is another way of indirectly referring to MEX 3D printing technology. In the following sections, material filament information and some simulation strategies would also be discussed, along with post-processing techniques. Many sections are explained in the context of the guidelines provided by BASF for their specific metal 3D printing processes, as a major part of this thesis involves using these guidelines and an Ultimaker S5 printer with a metal expansion kit. Therefore, more emphasis is put on understanding and stating these recommended guidelines by BASF. Nevertheless, the necessary other information is also provided.

3.1 Material Extrusion 3D Printing

MEX is one of the most popular Additive Manufacturing (AM) technologies. It gains its popularity from the fact that it can be used to produce complex designs that are not possible with traditional manufacturing. The technology could be simply described as follows: a 3D CAD file is converted into a STL file, which is then fed into a slicer software that creates a G-code from it. G-code files are, basically, a long sequence of machine instructions used by the actual printer. Following these instructions, the printer heats up the nozzles to melt the filament, which is then extruded and layered on the build plate. These layers of the chosen material are accurately stacked together to form the final shape as per the initial 3D CAD file. In the world of 3D printing, this technology is also referred to as FFF or Fused Deposition Modeling (FDM). In essence, both FDM and FFF describe the same 3D

printing technology and process as MEX. The difference is that FDM is a proprietary term, FFF is a more generic term, and MEX is defined according to the international standard ISO/ASTM 52900 [23]. In the document ahead, the term MEX 3D printing is used synonymously with FFF or FDM technology.

MEX 3D printing is widely used for both hobby and industrial purposes. It has a wide range of applications in prototyping due to its ease of printing and low cost of producing parts. Thermoplastics such as PLA, ABS, and many others are widely used in MEX 3D printing.

3.2 Metal Material Extrusion 3D Printing

This thesis deals with metal MEX 3D printing, a relatively new field compared to the other 3D printing technologies. Printing with metal in MEX technology works in a similar manner to printing with thermoplastic. Instead of the thermoplastic filament, a metal-polymer filament is used, which is a mix of a binder material and metal powder. For example, the BASF 316L is a mixture of 10% wt. thermoplastic and 90% wt. 316L metal powder. The thermoplastic works as a binder and stabilizes the extruded material to form a three dimensional shape.

The printed parts are called green parts, and further processing is needed for them to become fully metal parts. The processing consists of two stages, namely Debinding and Sintering. In the Debinding stage, the thermoplastic material is removed from the green part to obtain what is knows as brown part. A brown part could be compared to a sand castle, where any disturbance to the part could drastically affect the shape of the part. This brown part is then put into a furnace for the Sintering stage, where the remaining metal powder is sintered. In this process, the metal powder granules fuse with the adjacent metal powder granules at very high temperatures. After the metal powder granules are fused together, the part is cooled to room temperature to obtain the final metallic part [17] (refer Figure3.1).

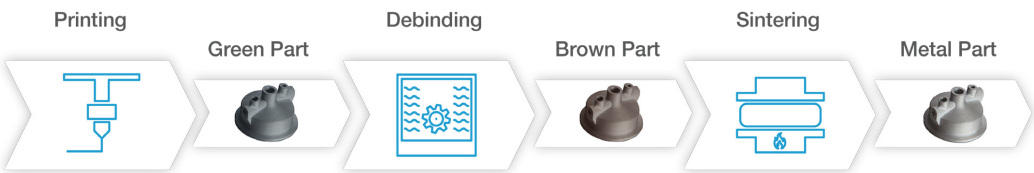

Figure 3.1: Metal Material Extrusion 3D printing process or metal FFF printing as per Ultimaker [17].

One of the advantages of metal MEX 3D printing is that a part could be further processed, when it is in its green state. For example, the part could be grinded or milled, or the green part could be surface polished to achieve a better surface

finish. This is possible because the part is polymer based which gives the user more flexibility to intervene and change the part as desired during the whole process. This is not the case in traditional manufacturing. This technology has made it very easy for everyone, even hobbyists to a certain extent, to print metal parts [17].

3.2.1 Debinding

Debinding is the process of removing the binder material from the green part. In the case of green parts printed with the S5, catalytic debinding is used to form brown parts. To debind the printed green part, BASF suggests that a catalytic debinding furnace with a gaseous acid environment of $HNO_3 > 98\%$ at 120 °C has to be used. An example of a debinding furnace is Nabertherm NRA 40/02-CDB [17]. For more information about debinding, refer [12].

3.2.2 Sintering

Sintering is a process in which a structure made of mainly metal powder is heated and sometimes also compressed so that the metal powder coalesces together without complete liquefaction of the metal. Just enough liquefaction takes place for the metal powder to fuse together [12].

When a part is metal MEX 3D printed and sent for the sintering process, it faces high anisotropic shrinkage, leading to different values of shrinkage in different axes. In the case of BASF metal-polymer filaments, the X and Y axis face the same level of shrinkage (16%), but the Z axis faces a larger amount of shrinkage (20%) compared to X and Y. During sintering, it is common to see warpage, especially in parts with a complex design. Symmetric parts shrink more homogeneously, and the distortion is much smaller [17].

As per BASF guidelines, the sintering needs to be done in 100% clean and dry hydrogen or argon atmosphere. The usual sintering process starts with heating the furnace at 5K/min until 600°C (873.15 K) is reached. The temperature is then maintained for one hour. Afterwards, with the same heating rate, the temperature is raised to 1380 °C (1653.15 K) and maintained at this temperature for another 3 hours. Lastly, the furnace is cooled down to bring the metal part, also called the white part, to room temperature. At the start of the sintering, the remaining binder is burned off. The binder constituents could have a fiber-like morphology as they contain MnO and manganosite. A special cleaning method should be used as the constituents could be hazardous to health [24].

3.3 Simulation

Metal MEX 3D printing can be an expensive process, and having several batches of failed parts is not an option in many cases. Simulating the part before printing and the D&S process cuts expenses as well as saves time, as the D&S process could take a long time, especially if the parts need to be outsourced for the D&S process. Below, a few of the simulation techniques are discussed as recommended by a white paper published by BASF [25].

3.3.1 Debinding Simulation

Debinding simulation is an important predictor of distortion and failure of the green part during debinding. It is also known as the brown part stability analysis. The main factor to be considered is gravity. During debinding, the gravitational forces of the part cause internal tensile and compression stresses. These stresses need to be considered when choosing the print orientation and design of the green part. BASF has some recommendations to perform a debinding simulation so that the structural integrity of the part could be achieved. These simulations help newcomers enter the technology and also help push the boundaries of lightweight design to drive down the cost of manufacturing [25].

Most of the CAD software with a finite element solver on the market could be used for debinding simulation, as it is a very basic gravitational force simulation. Software like Siemens NX, Solidworks, and Autodesk Inventor could be used. Some of the simulation assumptions and model conditions to be followed are stated below:

1. The print was ideal, that is, it does not have delamination, warpage, or porosity.
2. The green part has 100% infill
3. Fixed constraints must be added where supports are present or supports must be added in the model.
4. D&S process has the same orientation as the printing orientation.
5. The part will break if the maximum tensile or compression forces are exceeded.

A linear elastic material model is applied to the part, and and a liner static analysis is performed. The material properties to be applied are as shown in the Table 3.1.

Table 3.1: Brown part material property [25].

Mechanical Property	
Young's Modulus E	210 GPa
Density ρ	4700 kg/m3
Poisson's ratio ν	0.4

It is recommended to plot the stresses in the X, Y and Z axis. Then, check for stresses which are within the limit given below:

- On the X and Y axes, the maximum tensile stress is +6kPa and the maximum compression stress is -7kPa.
- On the Z axis, the maximum tensile stress is +0.5 kPa and the maximum compression stress is -7 kPa.

If the maximum threshold is exceeded on any axis, the debinding process will have a higher probability of failure, and cracks will be seen in the brown part. If during the part simulation the part fails, the following recommendations are provided by BASF to avoid cracks in the brown part [25]:

- The printing and D&S process orientation could be changed.
- The areas with large stresses could be redesigned by increasing the thickness of thin parts or adding chamfers on sharp edges to avoid stress concentrations.
- Keeping the parts smaller that 100 x 100 x 100 mm, will also help as the gravitational forces will decrease.
- Increase supports or add the supports to the model for a more realistic simulation.

3.3.2 Orientation Simulation

Many times, changing the design of a part is not possible. In such cases, the orientation of the part during the printing and D&S process is very important. Orientation simulation is not so different from Debinding simulation. It only involves changing the orientation of the part. All the other conditions remain the same as those of the debinding simulation. An orientation of the part is sought where the

minimum internal stresses are present. For simple parts, an educated guess for the orientation could work, but for a complex part, the orientation simulation could help provide a not-so-obvious orientation where minimum internal stresses are present [25].

3.3.3 Sinter Simulation

BASF does not provide much information on the sintering simulations they perform. They provide a service for their customers where they can perform the simulation for them. Software like LiveSinter could be used to perform in-house sintering simulation and compare the results to those after the D&S process.

3.4 BASF Metal-Polymer Material Filaments

BASF provides 2 metal composite filaments for printing metal parts. It also provides an support material (Ultrafuse®Support Layer) specifically designed to be used with BASF metal-polymer filaments. In the following subsections, a brief introduction to the filaments is given.

3.4.1 Ultrafuse®316L

BASF Forward AM Ultrafuse®316L filament (316L) is BASF's first metal-polymer composite filament available on the market from July 2019. The components printed with this filament can produce stainless steel (SS) type 316L after D&S process. BASF does not specifically list the components of the binder; however, the polymers used in the binder are a mixture of POM, polyacetal, and polyolefin [26]. Binder is used so that the filament could be melted and flow evenly during the green part printing stage. Also, it gives the filament flexibility to be used by any commercial MEX 3D printer using a bowden tube or direct drive extruder. The composition of the filament is 90% wt. powder and 10% thermoplastic polymer [17].

The approximate composition of the 316L SS part after sintering is given in the Table 3.2.

Table 3.2: Chemical Composition of sintered 316L part [14].

C%	**Cr%**	**Ni%**	**Mn%**	**Mo%**	**Si%**	**Fe%**
≤ 0.03	16-18	10-14	≤ 2	2-3	≤ 1	Balance

A few mechanical specifications of the 316L SS, as given by BASF, are given below in the Table 3.3:

Table 3.3: Material Properties of sintered 316L part [14].

Build Orientation	**XY**	**ZX**
Tensile Strength R_m	561 MPa	521 MPa
Elongation at Break ε	53 %	36 %
Yield Strength $R_{p0.2}$	251 MPa	234 MPa
Vickers Hardness HV 10	128	128
Density	7850 kg/m3	

3.4.2 Ultrafuse®17-4PH

BASF Forward AM Ultrafuse®17-4 PH filament (17-4PH) is BASF's second metal-polymer composite filament, released in December 2020. It is much stronger and harder than 316L. The parts printed using this filament produce SS type 17-4PH after the D&S process. It also uses a similar binder to that of 316L. It is not as flexible as 316L filament but can still be used for most MEX 3D printers with bowden tube or direct drive extruders.

The approximate composition of printed parts after D&S process is given in the Table 3.4 below:

Table 3.4: Chemical Composition of sintered 17-4PH part [15].

C%	**Cr%**	**Ni%**	**Cu%**	**Nb%**	**Mn%**	**Si%**	**Fe%**
≤ 0.07	15-17.5	3-5	3-5	0.15-0.45	≤ 1	≤ 1	Balance

The mechanical properties of 17-4PH are given in the Table 3.5. This data, based on tests from BASF, is relative to milled flat tensile bars with the shape E2x6x20 according to DIN 50125 [27]. The standard for testing is the same as for 316L, ISO 6892-1 [28].

Table 3.5: Material Properties of sintered 17-4PH part [15].

Print Direction	**XY**	**ZX**
Tensile Strength R_m	990 MPa	1004 MPa
Elongation at Break ε	4 %	4 %
Yield Strength $R_{p0.2}$	756 MPa	764 MPa
Vickers Hardness HV 10	291	309
Density	7600 kg/m3	

Furthermore, BASF also released data for mechanical properties of 17-4PH after H900 heat treatment. According to the data released by BASF, all the properties mentioned in Table 3.5 were increased by considereable amount after H900 heat treatment [15]. As per standard ASTM A564, to perform H900 heat treatment on 17-4PH part, a furnace is heated to a temperature of 900°F (approximately 482°C), and the temperature is maintained for 1 hr in the furnace, and then the part is cooled in air.

3.4.3 Ultrafuse®Support Layer

BASF Forward AM Ultrafuse®Support Layer (support material) is a composite filament containing mostly POM. This polymer is a semi-crystalline thermoplastic that has good sliding characteristics. It is commonly used as a binder for MIM parts. The filament is used as interface between two metal filament surfaces. This is done so that the metal surfaces don't fuse with each other during the sintering process. It is recommended to use this filament in a ventilated room or use a filter system, as during printing a small amount of formaldehyde is formed. This could be hazardous for health [12], [20].

3.5 Post-Processing

One of the major advantages of this technology is the machinability of the parts, both in their green state and after the sintering process. The green part is not as hard as the final sintered part. In this state, the part could be easily machined. For

example, the surface quality of the part could be increased by polishing or cutting. This reduces the cost of post-processing as any post processing after the part has been sintered would consume much more time and require better equipment. This could make the cost of producing parts cheaper, which in turn makes it easier to manufacture metal parts inhouse.

The final part could also be post-processed if any specific properties are needed, such as a very smooth surface finish or different surface properties. Examples of post processing could be heat treatment, milling, coating, and polishing. In short, it can be said that this technology is developed such that the final sintered part tries to closely resemble a metal part made by other traditional manufacturing processes. Therefore, any post processing that could be performed on a traditionally manufactured part could also be performed on the final sintered 3D printed part. [17].

3.6 Surface Roughness

Traditionally, surface roughness was measured using a sharp needle and running the needle across a surface to measure the change in topology of the surface. In this way, a 2D profile of the surface could be obtained. Various profile parameters were defined to characterize and analyse the surface, such as Ra, Rz, Rq, etc.[29]. With the recent developments in computing power, optical measurement devices have been developed to measure the 3D surface texture. New areal parameters such as Sa, Sz, etc. were defined to characterize the 3D data. These parameters were, in essence, extensions of the 2D parameters. Direct correlation between the 2D profile parameters and the 3D areal parameters might be possible; however, this topic is still under research [30]. Therefore, the conversion of 2D parameters to 3D parameters should be done with caution.

Following are the basic introductions to the parameters used in this thesis according to the new international standards for surface texture [31].

3.6.1 Sa

This parameter defines the arithmetical mean height of a surface as shown in Figure 3.2. It is an extension of Ra, which is the arithmetic mean height of a profile.

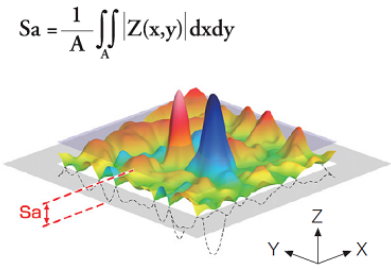

Figure 3.2: Pictorial example of Sa [32].

3.6.2 Sz

As a parameter, Sz is the sum of the maximum peak height and the maximum pit depth as shown in Figure 3.3.

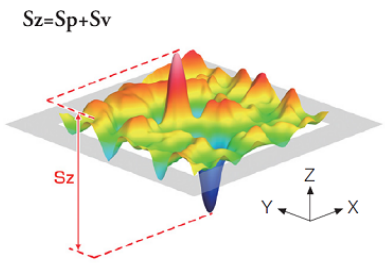

Figure 3.3: Pictorial example of Sz. Sp represents highest peak and Sv represent deepest pit [32].

3.6.3 Ssk

The skewness of the surface is defined by Ssk, which gives knowledge about the asymmetry or symmetry distribution of height (refer Figure 3.4). It presents insight into the texture morphology of the surface. Generally, a negative skewness value represents deep pits and plateaued surfaces. A positive skewness value represents shallow pits and high peaks on the surface.

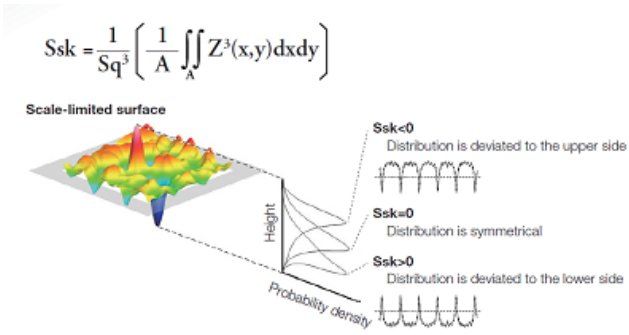

Figure 3.4: Pictorial example of Ssk [32].

3.6.4 Sku

The kurtosis of the surface is defined by Sku. Generally, this parameter provides knowledge of the sharpness of the peaks on the surface (refer Figure 3.5). A significantly smaller kurtosis value than 3 indicates that heights are spread more or less uniformly on the surface. A significantly higher kutosis value than 3 means that the distribution of heights is uneven and the surface has large peaks [33], [34].

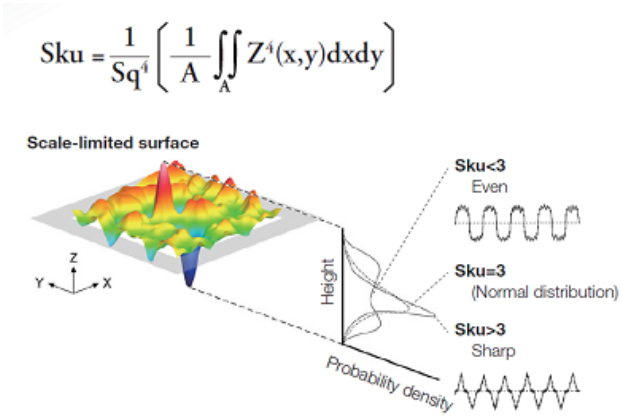

Figure 3.5: Pictorial example of Sku [32].

The kurtosis and skewness are very sensitive to error due to higher order mathematical equations [33]. The equations could be seen in Figures 3.4 and 3.5.

Chapter 4

Experiments

This chapter focuses on the experiments done in this study. It begins with explaining the equipments used, followed by a design of experiments. The execution procedure for all the experiments is also described. Lastly, the initial fabrication experience of the specimens is described.

4.1 Equipment

This section explains the regularly used equipments during this study to print green parts and measure data.

4.1.1 Ultimaker S5

In this thesis, Ultimaker S5 (S5), as seen in the Figure 4.1, was used for 3D printing the metal-polymer green parts. The specifications of this printer are given in Table 4.1.

The S5 is a desktop 3D printer, and it was equipped with an Ultimaker S5 Air Manager which encloses the printer from top so that the temperature inside the printer could be consistent. This reduces the probability of warping in the 3D printed parts. Further, the air coming out of the enclosed chamber is also filtered for toxicity and ultrafine particles. Figure 4.1 shows the attached Air Manager accessory for S5 [37].

This printer was also extended to print metal filament by using a Metal Expansion Kit provided by Ultimaker. This kit comes with Ultimaker certified 17-4PH and

Table 4.1: Specifications of Ultimkaer S5 printer [35].

Printer Property	**S5 Specifications**
Build Volume	Single Wall Calibration
Print head	Dual extrusion print head
Compatible filament diameter	2.85 mm
Layer resolution	0.4 mm nozzle: 200-20 μm
Nozzle diameters	0.4 mm
Nozzle temperature	180 - 280° C
Build plate	Glass build plate

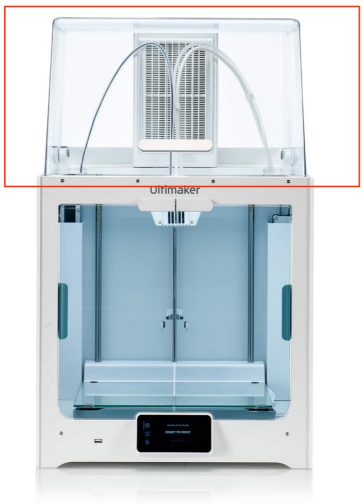

Figure 4.1: Ultimaker S5 [36]. The red box indicates the Air Manager.

Ultimaker certified support material. It also includes two Ultimaker print cores - CC and DD. The CC print core is an abrasion-resistant hardened steel nozzle and DD print core has a sapphire insert at the nozzle for abrasion-resistance. Print Core DD was specially designed for the support material [35], [38], [39].

4.1.2 Tensile Test Machine

Shimadzu AG-X is a hydraulic universal testing machine used for static material testing. This machine has real-time auto-tuning capabilities for more flexibility in testing. The force transducers (load cell) in the machine has an accuracy class 1 and

data sampling time of the machine is up to 10 kHz. This makes Shimadzu AG-X highly accurate and well suited to make stress-strain graphs. The maximum load capacity is 10 kN [40].

4.1.3 Surface Roughness Machine

A Nanovea PS50 profilometer was used in this thesis to record the surface roughness data. It is an optical non-contact profilometer using Chromatic Confocal technology. In this technology, white light passes through sphero-chromatic lenses and splits into different wavelengths. These light rays with different wavelengths have different vertical focal points, which are used to create a vertical measurement range. When a surface of interest comes into focus, some of the wavelengths of the white light will be in focus and others will not. This will make the in-focus wavelength pass through a pinhole to reach the Charge Coupled Device spectrometer, and finally the vertical position can be detected. For more in-dept information about the technology refer [41].

4.2 Design of Experiments

Design of Experiments (DOE) is a statistical method to determine the relationship between variable parameters (inputs) and the output of the experiment in a structured and planned manner so that any variation in the input parameter could be related to the output. The variable parameters or factors are selected, and different "levels" are defined to study the effect of these levels on the output of the experiment.

The basic method of DOE is a full factorial DOE, where one factor is changed through different levels and other factors are kept constant. Usually, DOE is used to decrease the number of tests planned to be executed when the number of factors is greater than 3. This kind of DOE is known as fractional factorial DOE [42]. In this thesis, the chosen factors are described in the subsections below.

4.2.1 Printing Orientations

It was hypothesized that the printing orientation would have an effect on the strength of the specimen, as the layers would get separated more easily if the tensile force direction and the printing direction were the same, as is in the case of thermoplastic MEX 3D printing. Also, as it can be seen from literature, printing orientations have an effect on the strength of materials [8]. Initially, for this thesis, three basic

orientations were chosen: XY, XZ, and ZX (refer Figure 2.1). As per BASF, the ZX orientation would be too unstable during the D&S process, and the specimen would crumble during the process. Therefore, only two orientations were considered for tensile testing, XY and XZ.

4.2.2 Surface Roughness

During printing, the surface parallel to the printing direction has layer marks (layered side). These valleys between layers could act as micro-notches and lead to earlier failure in the specimens. Thus, to investigate how these layers affect the strength of the material, polishing was chosen as a variable parameter. Two type of polishing were chosen for the specimens. One was with no polishing at all (as-printed), and one was with polishing on the sides parallel to the printing direction, with a polishing paper grade 150.

4.2.3 Printing Material

BASF provides two metal-polymer filaments: 316L and 17-4PH SS. These two materials were chosen to investigate their strength with respect to change in orientation and surface roughness. These two materials were selected as both are produced by the same manufacturer and recommended by Ultimaker to be used on their Ultimaker S5 3D printer. Both materials have 90% wt. metal powder, and the remaining 10% wt. is polymeric binder.

4.2.4 Full Factorial Design of Experiments

The above mentioned 3 factors were chosen at 2 levels with the full factorial method. Thus, 2^3 experiments were performed. A table is built consisting of all the experiments where one factor iterates through different levels. A 2-level DOE is one where +1 (high level) and -1 (low level) indicate the levels of the factor. For example, if the surface roughness of the samples is considered as a factor, the two levels are polished samples and unpolished samples. The +1 would indicate polished samples, and the -1 would indicate unpolished samples [42].

After the initial fabrication of specimens, it was observed that the on-edge tensile bar (see Figure 2.1 for naming conventions) had cracks during the D&S process. Due to this, printing orientation was eliminated from the DOE, and more efforts were focused on fabricating an on-edge tensile bar without any cracks for the rest of the thesis. As a result, the number of experiments was reduced to four. Each

experiment type was repeated three times so that a considerable sample size could be used and reliable data could be produced.

The following table (Table 4.2) of full factorial DOE represents the planned experiments in the study relating to two factors: factor A, representing surface roughness in the table; and factor B, representing material of the specimens in the table.

Table 4.2: Full Factorial Design of Experiments.

	Full Factorial	
	A	B
1	-1	-1
2	1	-1
3	-1	1
4	1	1

On the other hand, for metallographic analysis, five specimens were chosen for investigation: three green parts (unsintered) and two sintered specimens. For the three green parts, one was 316L, the second was 17-4PH, and the third was a layered specimen consisting of two layers of separate material: 316L and 17-4PH (refer Figure 4.2). For the sintered specimens, one was produced using 316L and the other was made of 17-4PH.

Figure 4.2: Layered sample in green state.

Towards the end of the study, a few extra tests were performed, including the 17-4PH green part tensile testing, which was not initially part of the DOE. One smaller version of an on-edge (XZ) tensile bar - having form E4x10x35 according to DIN 50125 - was also tested, after having been successfully sintered.

4.3 Specimen Design

The specimen design is one of the most important factors, as it determines the shape and weight of the specimen. The shape can impact the printability, and the weight affects how much material is used. For the tensile test, a flat tensile bar was chosen instead of a round one. Although it is true that the round specimens would have a better stress-strain curve due to uniform stress distribution, a flat specimen is chosen as the design has better and simpler printability. Another reason to use a flat specimen was to have comparable specimens to those of BASF and other research papers. The standard used by them for specimen design is DIN 50125 [27] and the testing was done according to ISO 6892-1 [28], which are the same standards used in this study.

At Rhine-Waal University of Applied Sciences, where tensile testing of the specimens was performed, the material testing lab made a few suggestions for the design parameters of the specimen according to their experience on the tensile testing machine. The following recommendations were given:

- The grip section should be 45 mm, as the grip holder in the tensile test machine is 40 mm.
- The gauge length should be 50 mm to get more accurate results.
- The thickness should be 3 or more mm so that the grippers could properly grip the specimen.

Taking into consideration the above recommendations and the DIN 50125 standard, the specimen dimensions were taken as shown in the Figure 4.3.

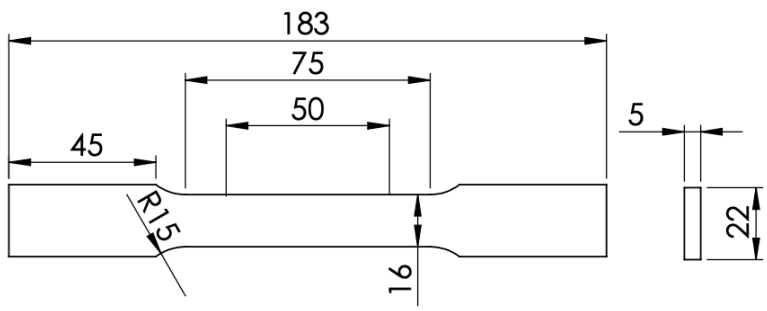

Figure 4.3: E5x16x50 form specimen according to DIN 50125

As 316L and 17-4PH specimens looked similar to each other after sintering, a very small chamfer was made on one end of the 316L specimens to differentiate them from the ones in the other material. This would not affect the tensile test, as the chamfer was done on the gripping area of the specimen. The size of the chamfer was 1 x 45 degrees. Further, a smaller specimen design was also made with smaller gauge length of 35 mm (see Figure 4.4).

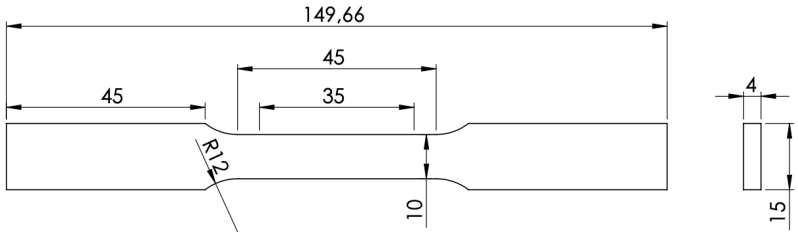

Figure 4.4: E4x10x35 form specimen according to DIN 50125

All the specimens were also milled on one side, specifically, the side in contact with the shrinkage plate as this presented a high surface roughness. The measured values of surface roughness, for the parameters Sa and Sz, in this rough surface were 19.63 and 202.33 μm, respectively. To avoid any cracks from this surface creeping into the specimen during the tensile test, 0.2 mm of material was milled from the horizontal tensile bar. The new surface roughness parameters, Sa and Sz, of the milled surface were 1.78 and 14.4 μm, respectively.

For metallographic analysis, five specimens of 10 x 10 x 50 mm dimensions were printed separately. Two were sent for the D&S process, and three were kept in their green state. The layered specimen was printed using one nozzle, and thus it was difficult to position the separation line between different materials at exactly 5 mm from the bottom. The separation line was approximately tried to be kept at 5 mm height from the bottom (refer Figure 4.2). This approximation does not affect the metallographic analysis.

The other two specimens that were sent for D&S process included one 316L specimen, and one 17-4PH specimen. Similar to the tensile test specimens, one side of the 316L specimen was chamfered.

4.4 Execution Procedure

In this section, the execution procedures for the different tests performed during this thesis are explained.

4.4.1 Shrinkage and Density

The printed specimens were measured with a vernier calliper (accuracy of 0.01 mm). All the measurement were performed three times, and the arithmetic mean was taken to get the final reading. For example, if the thickness of the sample is to be measured, then the sample was measured three times: once on either side and once in the center. After this, the arithmetic mean was taken to give the final thickness of the sample.

First, the green parts were measured. When green parts were measured, the thickness of the sample could not be directly measured due to the presence of the shrinkage plate as seen in Figure 4.5. Hence, it was calculated indirectly using the total thickness and thickness of the shrinkage plate measurements. For length and width, direct measurements were taken.

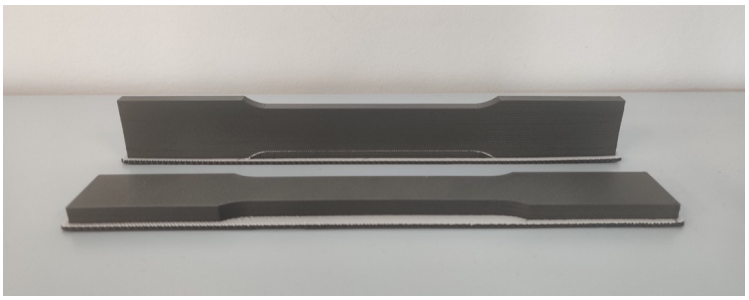

Figure 4.5: Specimens in the green state.

After the parts were received from the D&S process, direct measurements of all dimensions could be taken as the shrinkage plate was no longer attached to the sample. Shrinkage was calculated using the following formula:

$$Shrinkage_i = \frac{D_{green,i} - D_{sintered,i}}{D_{green,i}} \tag{4.1}$$

where i indicates the dimension of the part in X,Y, and Z axis. In the formula, D_{green} represents the dimension of the part in the green state, and similarly, $D_{sintered}$ represents the dimension of the part in the sintered state.

Two types of densities were calculated in this study. The description for each of them is as follow:

- Theoretical Density (ρ_{theo}) : To calculate ρ_{theo}, mass was measured using a weighing scale, while the theoretical volume of the part was noted from 3D CAD software Solidworks where, the specimen was designed. Finally, the following formula was used to calculate the theoretical density:

$$\rho_{theo} = \frac{M}{V_{theo}} \tag{4.2}$$

  where M depicts the mass of the specimen and V_{theo} depicts the theoretical volume. ρ_{theo} was measured for both green as well sintered parts

- Density (ρ_{wd}): To calculate ρ_{wd}, the Archimedes principle was used, also known as the water displacement method of calculating density. The volume of the sample was measured by putting the sample in the water and nothing the difference between initial and final level of water. The mass was measured with a weighing scale. Lastly, the following formula was used to calculate ρ_{wd}:

$$\rho_{wd} = \frac{M}{\Delta V} \tag{4.3}$$

  where ΔV depicts the change in volume after putting the specimen in water. ρ_{wd} was measured for only sintered parts.

4.4.2 Tensile Test

The tensile test was performed with a Shimadzu AG-X (see subsection 4.1.2) and according to ISO 6892-1. The stroke rate used in the testing was initially set to 0.5 mm/min for the first polished specimen of 316L, as this was similar to the value of 0.3 mm/min used by BASF for their tensile testing. However, it was evident that the level of accuracy given by this stroke rate was only needed for the elastic zone of the stress-strain curve. After this, a higher stroke rate could have been used. Therefore, referring to the values used by BASF (0.3 mm/min until 2% strain and 10mm/min until break), the stroke rate was updated to be 0.5 mm/min until 2% of the extensometer strain. After this point, 10 mm/min was instead used until the specimen breaks (refer to Figure 4.6). The 0.5 mm/min stroke rate was kept the same as the initial value to ensure that the conditions for the first 316L specimen and the ones tested after it were the same in the elastic zone. Therefore ensuring more comparable results. Lastly, three parameters were extracted from the data of the tensile test: Yield Strength (Rp0.2), Tensile Strength (Rm), and Elongation at Break (ε). In the documentation, fracture strain also refers to ε.

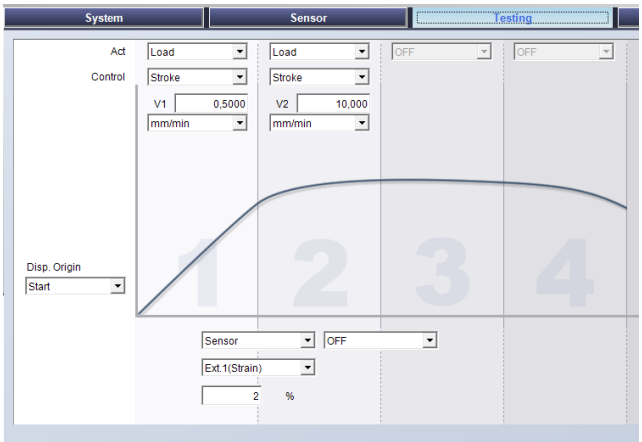

Figure 4.6: Stroke rate used in tensile testing.

4.4.3 Surface Roughness

The surface roughness was measured using a Nanovea PS50 profilometer (refer subsection 4.1.3). Areas of 1x1 mm were chosen on the specimens for analysis. To hold the specimen in place, a small vice was used as shown in the Figure 4.7. This ensured that the specimen was held on one of its sides, as due to the shrinkage plate, the specimens were not stable on their own when kept in XZ orientation. A small L-shaped plate was fixed to the workbench so that the vice or the specimen could be anchored in the L-shaped corner. This would ensure the same position for all the specimens.

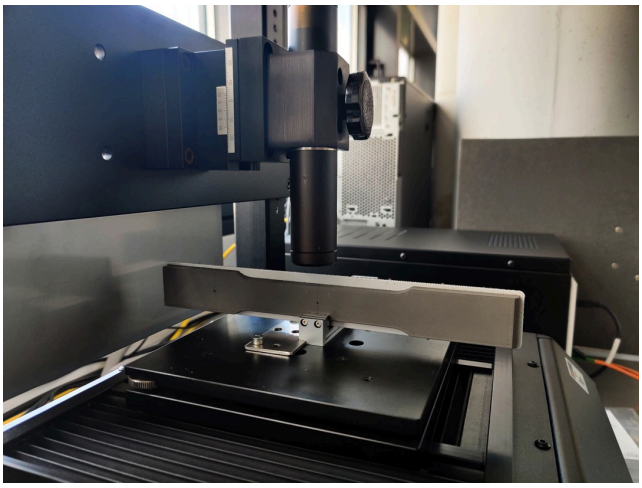

Figure 4.7: Nanovea PS50 profilometer workbench with a vice holding a specimen.

Surface roughness was measured before sintering, that is, on the green parts, and after sintering. This was done to understand the change in surface roughness before and after the D&S process. Four 1 x 1 mm areas on the specimens were chosen on the specimen to measure and collect surface roughness data. The center points of these areas are shown in Figure 4.8. Two points were chosen in the center of the specimen, one on the front face and one on the top face. Other two points, again one on the front and one on the top, were chosen at 7 cm from the center of the specimen. The chosen value of 7 cm is arbitrary. After the D&S process of the flat tensile bar, the point that was at 7 cm from the center, in the XY plane, would be now approx 5.88 cm away from the center due to 16% shrinkage [17].

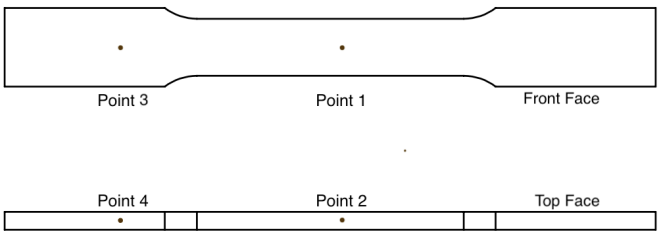

Figure 4.8: Points depicting the centers of areas selected for surface roughness measurements

4.4.4 Metallography

The metallographic analysis was carried out at Dr. Sommer Werkstofftechnik GmbH in Issum, Germany. For analysis of the microstructure of the material, the first step was to separate a section of the sample to be analyzed from the entire sample. This is known as sampling the material. Two sections from each specimen were taken using an abrasive cutting method. One section was parallel to the length of the specimen (lengthwise specimen), and the other was perpendicular to the length of the sample (crosswise specimen). This was done to analyse the difference in structure along different planes in the specimens.

The second step was to embed the sections in an epoxy holding device using hot moulding. The third step was to mechanically grind and polish the mounted specimens using wet grinding process (3 and 9 micrometrer diamond suspension liquid). Finally, the mounted specimens are cleaned with ethanol and water.

After cleaning, the specimens are ready to be analysed under an optical microscope. At this stage, pores, cracks, contamination, or corrosion attacks could be observed under the microscope. Usually, no microstructure is visible as the light is reflected back uniformly. To see the microstructure of the specimens, etching of the specimens need to be performed.

To take a look at the microstructure of the specimens, the sintered specimens were etched with a V2A etching solution. A V2A solution is a combination of hydrochloric acid, nitric acid, and distilled water. The green specimens were not etched as they would not result in any changes in the inspection under the microscope. For further analysis of the microstructure in the 316L sample, Murakami etching solution was prepared to detect sigma phase in the microsection [43]. Murakami solution is a combination of potassium ferricyanide, sodium hydroxide, and distilled water.

In the end, spot analysis was performed on areas of interest using Energy-dispersive X-ray Spectroscopy (EDX) analysis to obtain elemental composition data. The EDX capabilities were inbuilt in the Oxford Instruments' Scanning Electron Microscope (SEM). Optical Emission Spectroscopy (OES) was also performed on the samples to obtain the chemical composition of 316L and 17-4PH.

4.5 Specimen Fabrication

In this section, experience with the initial prints and printing of the specimens will be explained.

4.5.1 Initial Fabrications

After initial setup of the S5 with the metal extension kit, some initial fabrications were done with the default 3D printing parameters specified by BASF in the Cura software. Some of the important parameters used in the Ultimaker S5 are given in Appendix Table A.1. Few simple shapes such as cubes and plates were successfully printed. The initial print was printed using Magigoo Metal Glue to improve adhesion to the build plate. To remove the parts from the build plate after printing, it is recommended to immerse the build plate in water for 1-3 hours to ensure the dissolution of the Magigoo Metal Glue. Other common methods to improve adhesion, such as 3DLAC Spray and Polyimide Film (Kapton film), were also tried but it was found that Magigoo Metal glue performed better. The kapton tape lost its adhesion property after one print in the spot where the part was sticking to it. On the other hand, 3DLAC Spray displayed similar adhesion properties as

Magigoo Metal Glue, and the green parts took a similar amount of time to come off the glass build plate.

4.5.2 Specimen Fabrication Trials

After the initial printing of green parts, more parts were printed, such as a simple ring and a ring with holes. This was to cross-check if the shrinkage was the same in the X and Y axes after the D&S process. Samples of flat tensile bars were also printed in horizontal (XY) and on-edge (XZ) orientations. These were printed in two sizes - E4x10x35 and E5x16x50, according to DIN 50125. This was done because the size of the E5 green part was more than 200 mm in length, because of which it had a higher probability of facing warpage while printing or cracking during the D&S process. Thus, a smaller size E4 specimen was also printed.

The green parts were sent for D&S processing to Elnik Systems GmbH, Germany. After the parts were received, most of them did not crack. The flat tensile bar had a very slight concave curve. The rings shrank approximately 16% in both X and Y axes. Confirming that both axes have similar shrinkages and that a circular hollow shape could be maintained even after the D&S process. The Z-axis shrinkage was approximately 19%, and according to BASF, around 20% shrinkage could be expected in the Z axis and 16% in the XY plane [17]. The same ring was printed with a conventional MEX 3D printer with PLA filament to compare it with the metal ring. It was noted that there were no large dimensional differences (0.2 mm accuracy) between the metal and PLA ring (refer Figure 4.9).

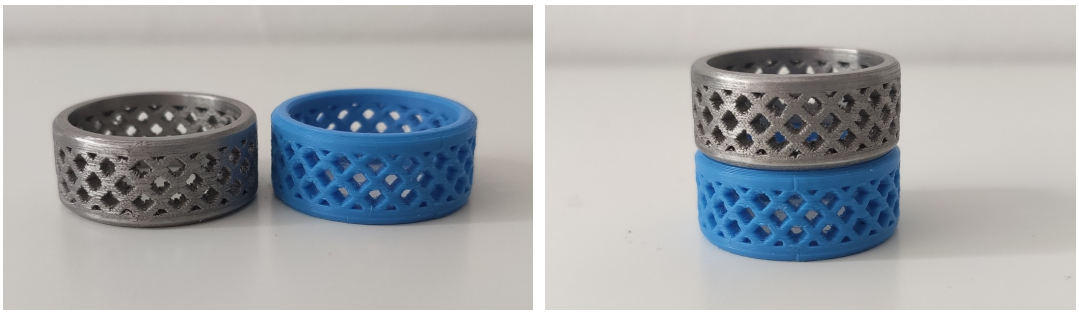

(a) Metal and PLA rings side by side. (b) Metal ring on top of PLA ring.

Figure 4.9: Metal and PLA rings. The metal ring is slightly polished.

The E5x16x50 part, printed in on-edge orientation, cracked after the D&S process as shown in Figure 4.10. Initially, it was hypothesized that the part cracked during the sintering process due to warpage, as the part had a slight concave curve when viewed from the side. Later, when the images from the D&S process were received,

it was seen that the part cracked during the debinding process, and then the cracks widened a bit more leading to warping during the sintering process.

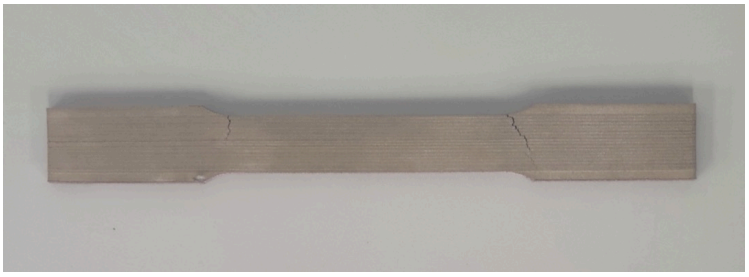

Figure 4.10: Cracked on-edge tensile bar. This is the first iteration.

When BASF was contacted regarding the cracked part, they recommended following a special guide specifically designed for troubleshooting defects of the green part to improve structural resistance during the D&S process [22]. When the troubleshooting guideline was followed and a new on-edge tensile bar was printed according to the changed parameters, the part warped during printing as shown in the Figure 4.11.

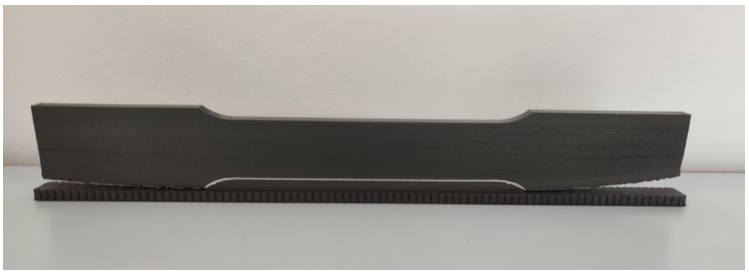

Figure 4.11: On-edge warped tensile bar after changing printing parameters as per [22].

It was deduced that the white interface layer did not have enough adhesion to the shrinkage plate. Hence, the white interface layer was expanded laterally to have more surface area to stick to the shrinkage plate. The white layer was made larger using the *Support Horizontal Expansion* parameter, which was set to 1.5 mm. A successful print was obtained after the change in parameter. Afterwards, the shrinkage plate was milled on the bottom surface in order to make it planar. This process was needed to ensure that no critical stresses could develop on the part during D&S, due to an uneven bottom surface.

The above change in settings, though, didn't seem to have the wished effect since the part still presented cracks after D&S (refer Figure 4.12). The part seemed to have

cracked again during the debinding process, although, the cracks were comparatively smaller with respect to the previous cracked parts. After further analysis of the part, it was observed that the part only touches the shrinkage plate in the center, when kept on the sintered shrinkage plate. If the part is pushed down the side, it lifts, pivoting on the center, confirming that the point of contact is, in fact, in the center.

Figure 4.12: Cracked on-edge tensile bar on sintered support. This is the second iteration.

Considering that the interface layer (0.45 mm thick) almost disappears during debinding and that a gap of 0.45 mm is left between the part and the shrinkage plate, uneven debinding could have caused the central portion of the specimen to be first in contact with the shrinkage plate. This could have induced critical stresses in the part, causing the development of cracks. One way to avoid cracks could be to reduce the interface layer thickness from 0.45 to 0.3 mm. This could increase the probability of realizing a more uniform contact between the part and the shrinkage plate. Due to time constraints, this hypothesis hasn't been tested. However, upon consultation with BASF, the hypothesis has been considered valid and further investigation is required.

Aside from the on-edge tensile bars, the flat tensile bar did not crack after the D&S process in the initial run; therefore, 12 additional flat tensile bars were printed as per the DOE and sent for D&S process.

4.6 Limitations of Experiments

This section discusses the general limitations and drawbacks with respect to the experiments and the collected data. Some limitations are stated below:

- Extreme care was taken to eliminate human error while measuring the data by taking an arithmetic mean of three values for each measurement. However, it was seen that the samples had sharp edges (similar to a metal burr), which

could exaggerate the measurements by a small value (approximately 0.1 - 0.2 mm). These measurements could have led to faulty shrinkage values in the printing direction (thickness measurements).

- The specimens received after the D&S process were very slightly curved due to warping. These could affect the strength properties of the materials.
- Density is measured using the water displacement method based on the Archimedes principle. However, the water beaker used for measuring change in volume had a accuracy of more than 1 ml, and this was determined to be too low for accurate calculation of density.
- 316L and 17-4PH do not have an upper yield strength or a lower yield strength. So, Rp0.2 was calculated to determine the yield strength. The process for doing this was to manually select two points in the elastic zone so that the slope could be calculated, and thereafter, the software would calculate Rp0.2. The same range was selected across all the specimens of a particular material. However, with a change in the interval, it was observed that the yield strength fluctuates by a small value and thus, the yield strength values in this study are not clearly defined as the tensile strength values.

Chapter 5

Data Evaluation and Discussion

This chapter compares and evaluates the data collected from testing and physical measurements. It goes through all the experiments as discussed in Chapter 4.

5.1 Visual Inspection

Manual visual scanning of the specimens was done to detect any easily detectable features in the printed and sintered specimens. Some interesting points noted were as follows:

- The printing quality of green parts for 17-4PH was better than 316L. This was attributed to the better flow of melted 17-4PH metal-polymer filament compared to melted 316L metal-polymer filament.
- The sintered specimens had a slight concave contour. This defect could be due to warping.
- The surface roughness of the contact surface with the shrinkage plate presented a very high roughness and was not uniform throughout the surface. A picture can be found in Appendix A.
- Smaller parts within the given recommendations of BASF had smaller defects such as warpage.
- 17-4PH specimens shrank more than 316L specimens after the D&S process. A picture can be found in Appendix A.

5.2 Shrinkage

The Figure 5.1 presents mean shrinkage percentages for length (X), width (Y), and thickness (Z). Further, error bars are plotted, which represent the maximum and minimum values in the sample space. The sample size for these measurements was 6, consisting of 3 polished and 3 unpolished samples. On average, it could be seen from the figure that the mean shrinkage values for length and width for 17-4 PH are higher than those of 316L. This could also be clearly seen in the length of all samples. Further, the error bars for length and width are also considerably small, instilling more confidence in the results. These values are also in accordance with the values provided by BASF [17].

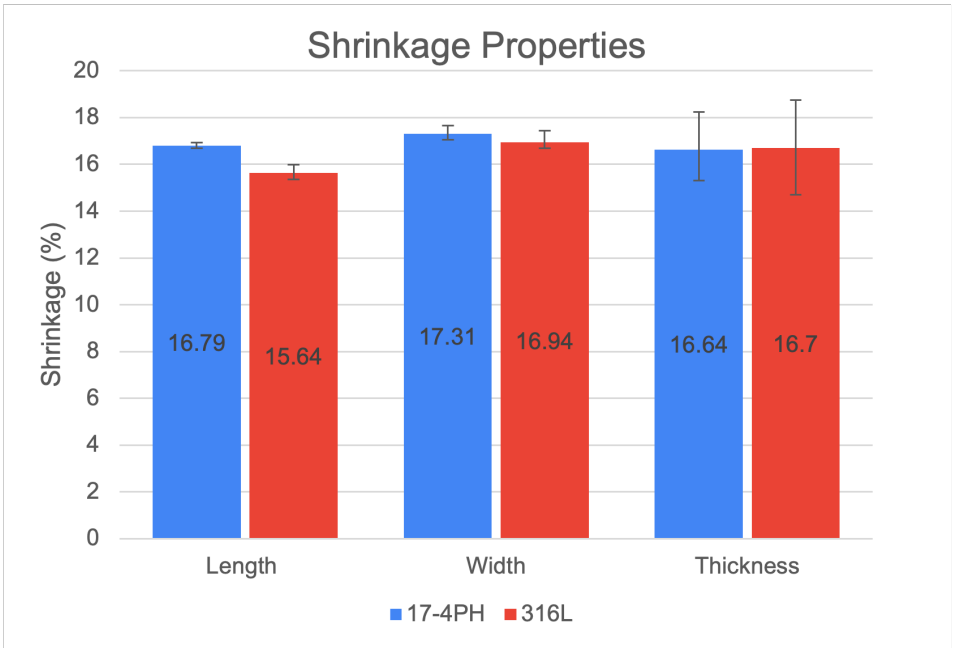

Figure 5.1: Shrinkage bar graph. Error bars represent the maximum and minimum values in the sample space.

Surprisingly, the values for shrinkage in thickness were almost 3% lower than the values provided by BASF. It is hypothesized that these could be due to taking measurements when the samples had a sharp edge, similar to a metal burr, around the boundary. This sharp boundary is caused by the contact between the shrinkage plate and the specimen. This could have caused the values of thickness to increase slightly more (around 0.1- 0.2 mm) than their actual values. In hindsight, grinding the sharp edges could have provided more concrete results. Furthermore, the large length of the error bar, almost 4%, in thickness shrinkage measurements indicates that they had a lot of fluctuations. In turn, decreasing confidence in the final result.

5.3 Density

The results of density measurements are given in the subsections below. The Theoretical Density (ρ_{theo}) of green parts is discussed, followed by the Density (ρ_{wd}) measured using water displacement method and ρ_{theo} of sintered parts.

5.3.1 Green Parts

The theoretical density of green parts was measured using a sample size of 6 specimens for each material, and the results are given in the Table 5.1. It can be inferred that 316L green parts are denser than 17-4PH green parts.

Table 5.1: Density of 316L and 17-4PH parts in green state

	316L	**17-4PH**
Theoretical Density $[kg/m^3]$	4877.92	4351.45

5.3.2 Sintered Parts

For the same set of specimens, density measurements were performed once again after the D&S process. Two different types of methods were used to measure density, and the results have been plotted in the same bar graph for comparison. Maximum and minimum values were also plotted in the form of error bars in the bar chart.

The results from density calculations are shown in the Figure 5.2. It can be concluded from this figure that the mean values of ρ_{theo} and ρ_{wd} are similar, but the error bars indicate the uncertainty in measurements of ρ_{wd}. This uncertainty could be due to the method used to measure the volume of the sintered parts. As described in subsection 3.3.1, water displacement method was used to measure the volume of the specimens. However, the accuracy of the beaker used to measure the volume change was greater than 1 ml. This accuracy is seen to be too low, and a higher accuracy is needed for measuring density. An alternative could be to use the change in mass of the specimen in water and in air to determine the volume of the specimen. Using the mass method is much more reliable and accurate, since devices used to measure mass at the milligram level are widely available.

The densities of 17-4 PH and 316L are 7650 and 7850 kg/m^3 respectively, as per the technical data sheet released by BASF [14], [15]. These values are in close proximity to the mean ρ_{theo} density values calculated in this study.

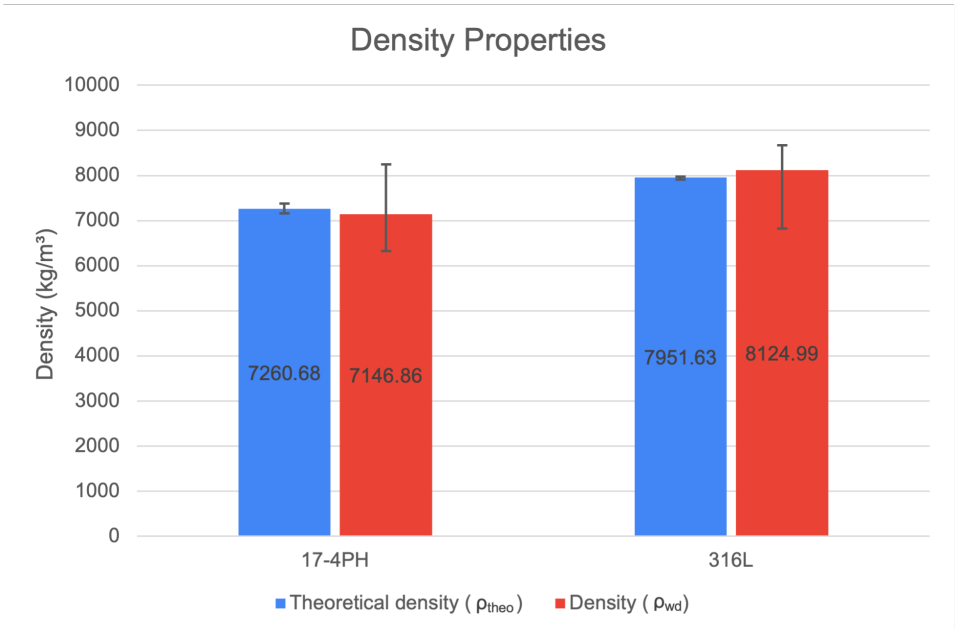

Figure 5.2: Density bar graph. Error bars represent the maximum and minimum values in the sample space.

5.4 Surface Roughness

The findings of the areal surface parameters Sz, Sa, Ssk, and Sku found on the specimens will be discussed in the following subsections. For general comparison, a part made via traditional manufacturing was taken and surface roughness was measured. A casted T-joint part was chosen for this purpose as shown in Figure 5.3. The measurements were conducted inside the smaller T-shaped region of the part.

Figure 5.3: Casted T-joint

The surface roughness parameters measured for this part are shown in Table 5.2

Table 5.2: Casted T-joint surface roughness parameters

	Sz [μm]	**Sa** [μm]	**Ssk**	**Sku**
Casted T-joint Part	20.46	7.9	-0.394	2.71

5.4.1 Unpolished Samples

The results of areal surface roughness for unpolished 316L samples are given in Figure 5.4. All four areal roughness parameter results of before and after the D&S process have been plotted in the figure. The naming convention of Front face and Top face could be seen in Figure 4.8.

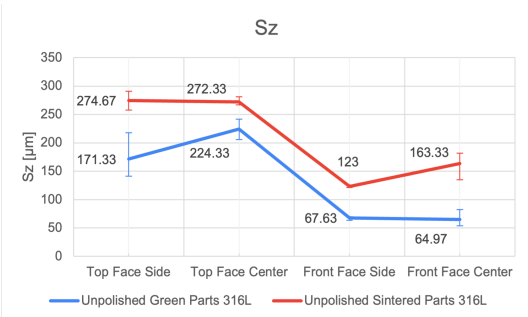

(a) Maximum height areal roughness parameter

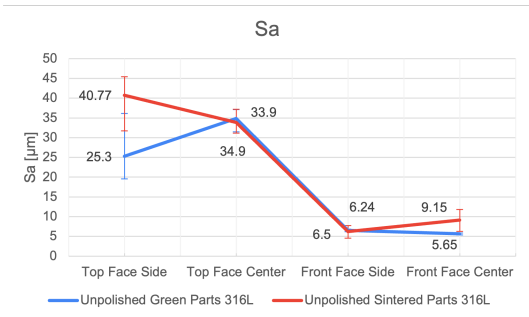

(b) Arithmetic average height areal roughness parameter

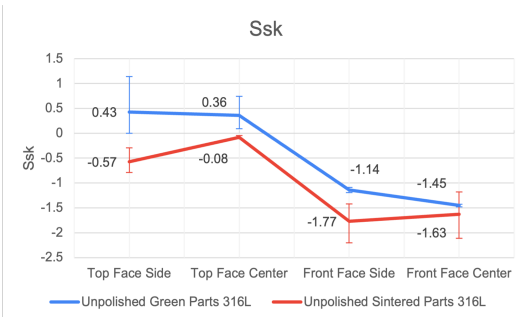

(c) Skewness areal roughness parameter

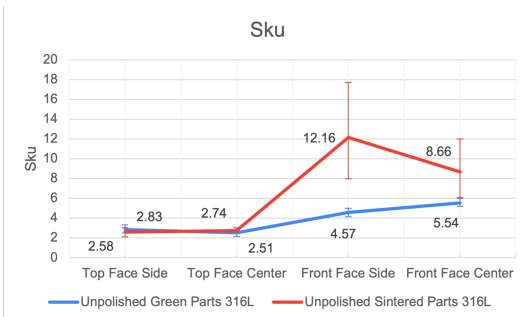

(d) Kurtosis areal roughness parameter

Figure 5.4: Surface roughness evolution in unpolished 316L specimens with the D&S process. Error bars represent the maximum and minimum values in the sample space

In general, it is observed that the roughness parameters increase after the D&S process, as shown in the plots of Sz and Sa. Significant changes in Sz values have been seen, and this could be attributable to the large shrinkage of the overall sample. A great difference is seen in kurtosis for front face values after sintering in comparison to the top face values. This indicates that there are more extreme heights present in the Front face comapred to the Top face. This might be because of different shrinkage levels in the printing direction (20%) as compared to the plane perpendicular to the print direction (16%) [17]. Further, the increase in negativity of skewness after the D&S process indicates an increase in the number of lower surface features (deep pits) in the surface of the specimen. This, in combination with an increase in Sz value, suggests that the surface gets more asymmetric, rougher, and has more pronounced extreme features after D&S process.

An overarching reason for drastic changes in the areal roughness parameters could be attributed to the large shrinkage the specimens go through during sintering and the disappearance of the binder. Lastly, the surface roughness measurements, Sa and Sz, were drastically higher for the specimens in this thesis compared to those of casted T-joint part.

5.4.2 Polished Samples

The four areal roughness parameters before and after the D&S process are plotted in the Figure 5.5. Similar to the results of unpolished 316L samples, an increase in areal roughness parameters was observed after the D&S process in the polished 316L specimens. Interestingly, a constant change was seen in all the Sz values. Positive skewness was converted into negative skewness, likely due to shrinkage. An increase in the sharpness of the peaks was also noted from an increase in kurtosis throughout all four measuring positions. No other special features in the plots were noticeable.

Overall, 17-4PH also exhibited similar behavior to 316L in the change of areal roughness parameters, apart from interesting plots for kurtosis as shown in Figure 5.6. In 316L, the kurtosis values grew after D&S process; however, in case of 17-4PH samples, the kurtosis values decreased after the D&S process. Especially in the polished sample, where all four data points showed a decrease in kurtosis values. However, the error bar in these graphs also shows a lot of uncertainty. Nevertheless, this is an interesting finding that could be explored more in the future. The Appendix A contains additional figures corresponding to other areal roughness parameters.

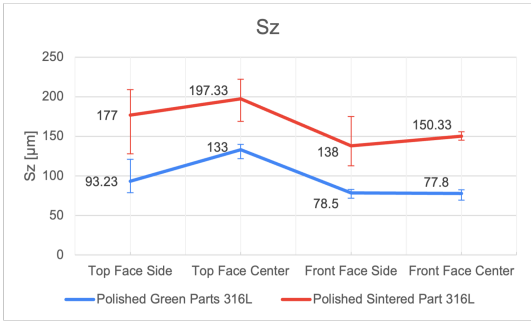

(a) Maximum height areal roughness parameter

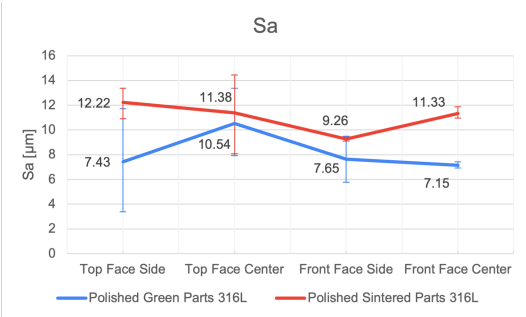

(b) Arithmetic average height areal roughness parameter

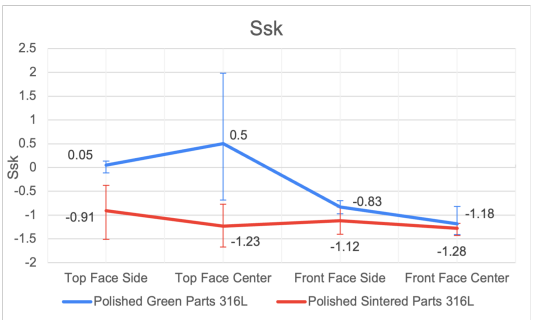

(c) Skewness areal roughness parameter

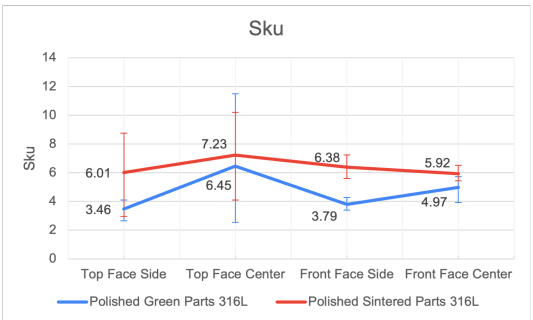

(d) Kurtosis areal roughness parameter

Figure 5.5: Surface roughness evolution in polished 316L specimens with the D&S process. Error bars represent the maximum and minimum values in the sample space

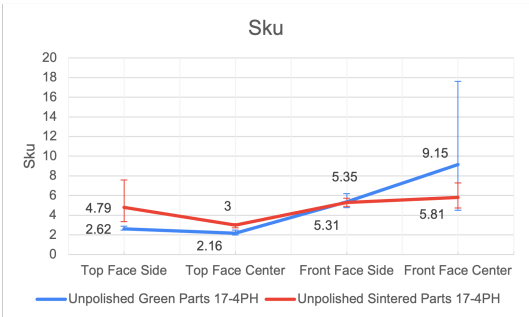

(a) Unpolished specimen

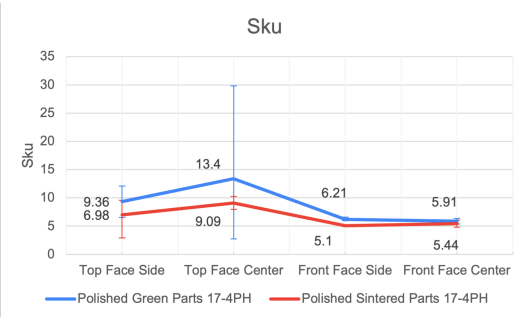

(b) Polished specimen

Figure 5.6: Kurtosis areal roughness parameter of 17-4PH specimens. Error bars represent the maximum and minimum values in the sample space

5.5 Tensile Test

The tensile test results for polished and unpolished 316L and 17-4PH specimens are shown in Figure 5.7. A sample size of 3 for each subcategory was used, and the values shown in the Figure 5.7 are the mean values. As in the previous bar graphs, the error bars indicate the maximum and minimum values in the sample space. Some similar interpretations could be obtained from both 316L and 17-4PH specimens. It can be seen that the unpolished and polished samples have similar tensile strengths, contrary to the hypothesis made in Chapter 1. Further, the polished samples are seen to have 15-20 MPa higher yield strength than the unpolished specimens. For 316L samples, this is an increase of approximately 7% and for 17-4PH samples, it is an increase of approximately 2.5 %.

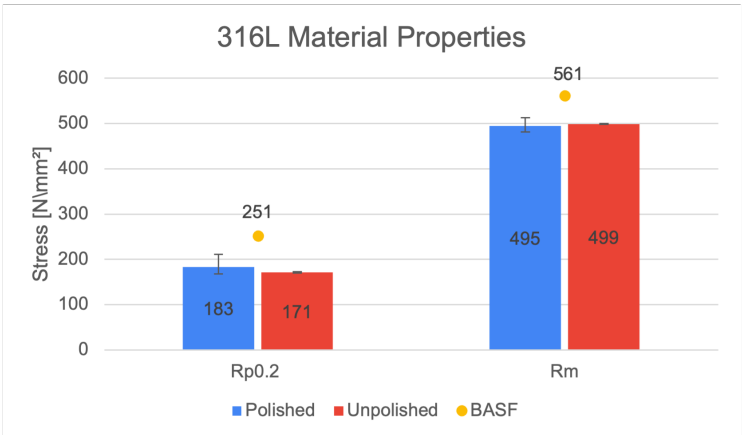

(a) Strength properties of 316L material.

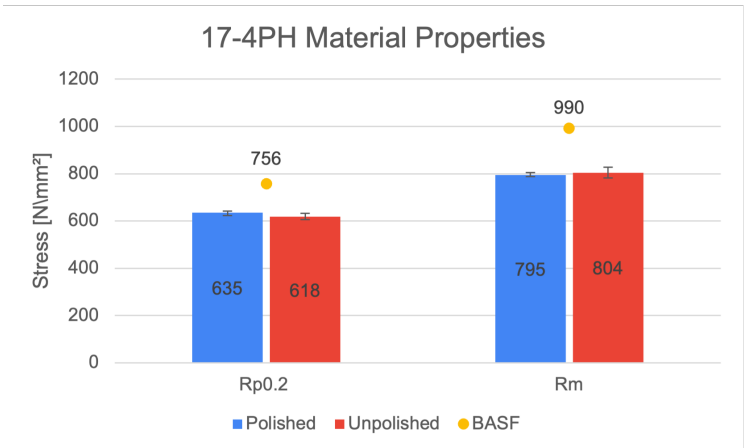

(b) Strength properties of 17-4PH material.

Figure 5.7: Strength properties of 316L and 17-4PH materials.

Furthermore, as seen in the Figure 5.7, the values released by BASF for their testing have significantly higher values than the results obtained in this study. In terms of yield strength, polished and unpolished 316L specimens have approximately 27% and 32% lower yield strengths, respectively, than the values given by BASF. Additionally, compared to the BASF provided tensile strength values, these values are about 12% lower for both polished and unpolished specimens. Similarly, for yield strength of 17-4PH, the values acquired in this study are 16% and 18% lower than BASF's yield strength values. Lastly, the tensile strength values are approximately 19% lower than BASF's tensile strength values. This could be attributed to the basic difference in specimens. BASF used specimens milled from a 3D printed block of material; however, the specimens used in this thesis, for example the unpolished specimens, are used as-printed with one side milled for tensile testing. Additionally, smaller geometrical deformations like slight curved samples due to warpage could have also played a part in lower strength values.

The strength results procured for 316L material in this thesis are in agreement with the results of a similar study [8] (refer Figure 2.3) and higher than those found in the study [5] (see Table 2.2). Furthermore, the results found in this thesis for 17-4PH tensile strength properties are higher than those found in studies [5], [7], and [10]. Custom 17-4PH filament was used in the study [10], while other studies [5] and [7] used Markforged 17-4PH metal-polymer filament.

Table 5.3 summarizes the mean fracture strain values. It could be observed that unpolished 316L samples had a higher fracture strain tolerance compared to polished 316L specimens. Comparatively, the values presented by BASF are higher than the values acquired in this study for both materials.

Table 5.3: Fracture strain [%] values of 316L and 17-4PH, along with released fracture strain values by BASF [14], [15]. The strain values are rounded off as per ISO 6892-1.

	316L Polished	316L Unpolished	BASF 316L	17-4PH Polished	17-4PH Unpolished	BASF 17-4PH
Fracture strain [%]	49	51	53	3	3	4

Comparing the fracture strain results of 316L and 17-4PH confirms the ductile behavior of 316L material and the brittle behavior of 17-4PH. This could also be seen in the necking of both materials after the tensile test, as shown in Figure 5.8. Large necking could be observed in 316L samples, whereas hardly any necking could be observed in 17-4PH samples.

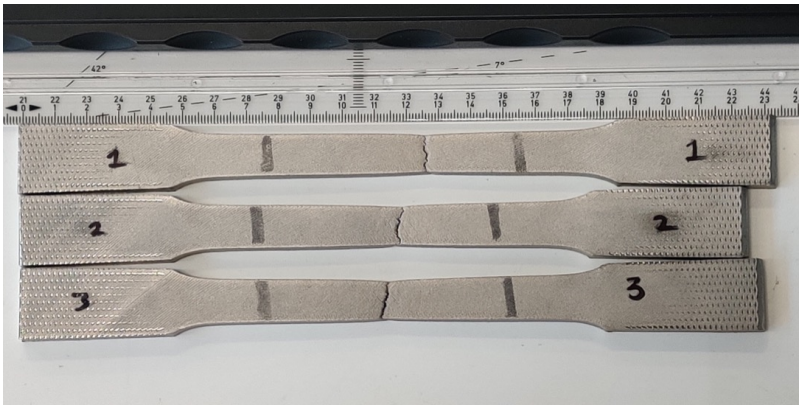

(a) Tensile tested 316L polished specimens.

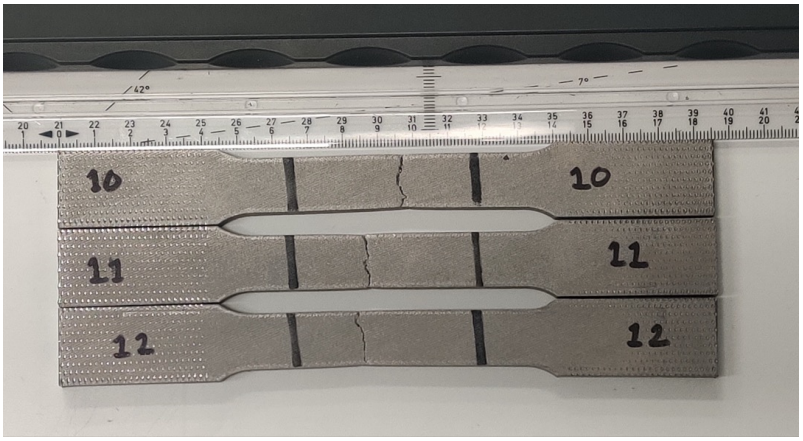

(b) Tensile tested unpolished specimens.

Figure 5.8: Tensile tested specimens showing necking.

5.5.1 17-4PH On-edge Unpolished Specimen

One sample of E4x10x35 survived the D&S process without cracking, unlike the E5x16x50 samples. Tensile test was also performed on this 17-4PH on-edge unpolished specimen to get a general idea of the material properties. The results of this test are shown in Table 5.4.

Table 5.4: 17-4PH on-edge unpolished specimen material properties.

	$R_{p,0.2}$ $[N/mm^2]$	R_m $[N/mm^2]$	ε [%]
17-4PH On-edge Unpolished	701	830	5

In comparison to the results of flat 17-4PH unpolished specimens, the on-edge specimen showed much higher yield strength and tensile strength, along with a higher fracture strain value. Unfortunately, BASF does not provide test results for this orientation. In a study [44], it was found that on-edge printed specimens were tested in an as-printed condition. In this research, Fused Deposition of Metals (FDMet) technology was used for the preparation of the samples. This technology comes under the umbrella term of MEX, and thus, this study could be used for comparison. The tensile strength was determined to be 840 MPa, which is also in accordance with results found in this thesis. However, values for flat printed bars were reported to be 880 MPa. These values are significantly higher than the values found in this thesis. This study illustrates that flat printed specimens are stronger than on-edge specimens. For more information, refer [44].

5.5.2 17-4PH Flat Unpolished Green Specimen

In this subsection, the results of the tensile test performed on a 17-4PH flat unpolished specimen in green state are presented in Table 5.5. The specimen had a form of E5x16x50. The table also includes tensile strength and elongation at break value of Ultrafuse PLA for comparison. The table has the values of specimens printed in flat orientation (XY).

Table 5.5: 17-4PH green part basic material properties. Ultrafuse PLA material properties extracted from [45].

	R_m $[N/mm^2]$	ε [%]
17-4PH Green Unpolished	7.8	11.4
Ultrafuse PLA	34.7	4.2

5.6 Chemical Composition

Optical Emission Spectroscopy (OES) was performed on the sintered 316L and 17-4PH samples to determine there chemical composition. The OES analysis was performed three times on each sample, and average values of the chemical composition were calculated. OES was also tried to be performed on the green parts made of 316L and 17-4PH. However, this procedure was not possible as green parts of 316L and 17-4PH were not electrically conductive. This could be because the metal powder in the green parts does not form continuous contact from one side

to another, or alternatively, the insulating properties of the binder material may have impeded the passage of the electrical current.

The averaged OES analysis results of 316L samples are as follows:

Table 5.6: OES analysis results of sintered 316L part.

C%	**Cr%**	**Ni%**	**Mn%**	**Mo%**	**Si%**	**Fe%**
0.0046	17.19	9.96	1.239	2.204	0.659	Balance

The above results match the chemical composition of 316L provided by BASF (refer Table 3.2).

The averaged OES analysis results of 17-4PH samples are as follows:

Table 5.7: OES analysis results of sintered 17-4PH part.

C%	**Cr%**	**Ni%**	**Cu%**	**Nb%**	**Mn%**	**Si%**	**Fe%**
0.0066	16.44	4.168	3.56	0.214	0.279	0.338	Balance

The above results match the chemical composition of 17-4PH provided by BASF (refer Table 3.4).

5.7 Metallography: Green State

The results of the metallographic analysis of green samples are presented in this section. Light Optical Metallography (LOM) analysis was performed on the green state samples of 316L, 17-4PH, and a layered sample of both 316L and 17-4PH. Crosswise and lengthwise sections were analyzed for 316L and 17-4PH green samples, and only crosswise sections was analyzed for layered samples. The 25x zoom micrographs of crosswise sections are shown in the Figure 5.9.

The white spots in the micrograph illustrate the metal powder, and the black zones are the binder. A lot more and smaller white spots are observed in the 316L micrograph than in the 17-4PH micrograph. This could also be clearly seen in the layered sample, where the top half corresponds to 17-4PH and the bottom half

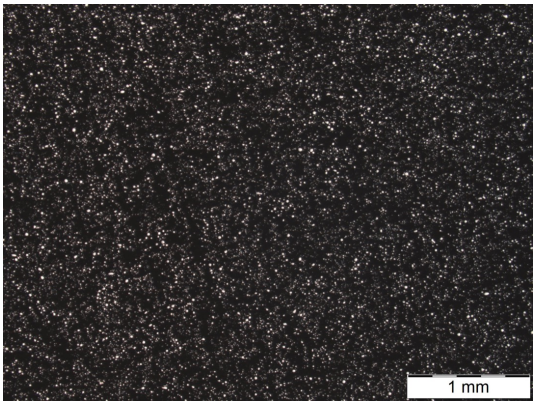

(a) Micrograph of 316L green sample

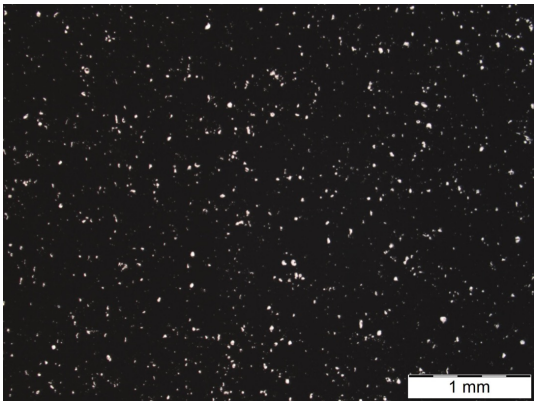

(b) Micrograph of 17-4PH green sample

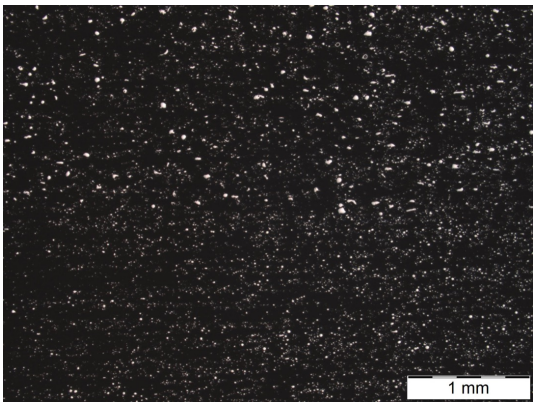

(c) Micrograph of layered green sample

Figure 5.9: 25x zoom micrographs of green state of crosswise samples

corresponds to 316L. However, it should be noted that due to the extreme brittleness of the samples, it was observed that it was extremely difficult to make the samples planar, and both samples should theoretically contain the same amount of metal powder, 90% wt. Nonetheless, this kind of pattern was also observed in all the other 25x and 100x zoom micrographs of green samples. No special difference was noted in the micrographs between lengthwise and crosswise section micrographs. The remaining 316L and 17-4PH lengthwise micrographs can be found in Appendix A.

5.8 Metallography: Unetched Sintered State

One unetched sintered sample of each 316L and 17-4PH material was analyzed. Two sections, lengthwise and crosswise, were taken from each material sample. The 25x zoom micrographs are shown in Figure 5.10.

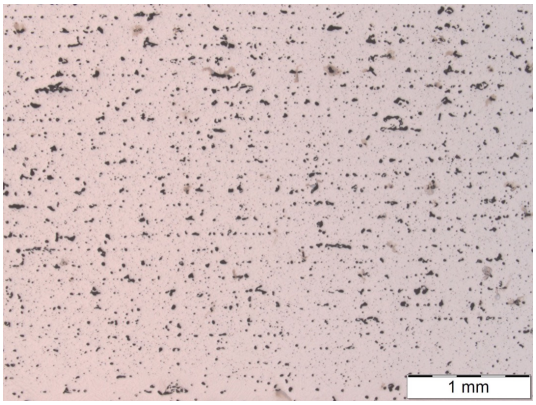

(a) 17-4PH lengthwise unetched section

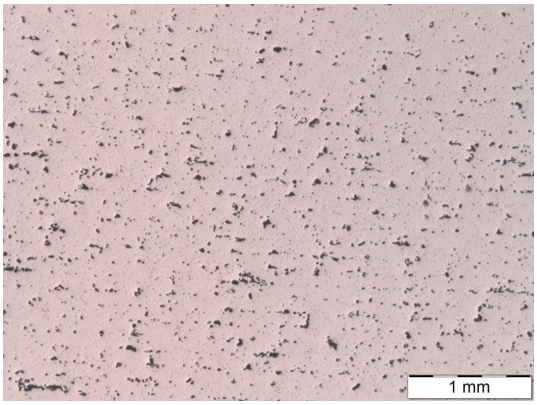

(b) 316L lengthwise unetched section

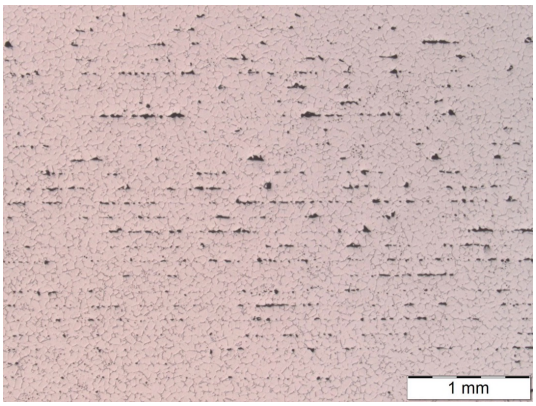

(c) 17-4PH crosswise unetched section

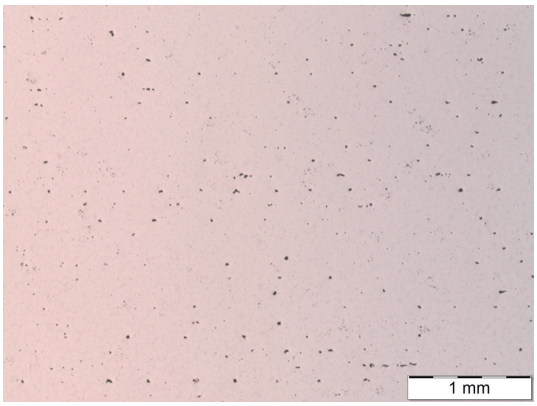

(d) 316L crosswise unetched section

Figure 5.10: 25x Zoom micrographs of unetched sintered samples

The first thing that stands out in all the micrographs in Figure 5.10 is the presence of voids, with more voids present in 17-4PH than 316L. Secondly, the printing layer directions could also be seen in lengthwise sections of 17-4PH and 316L. Also, very less voids were observed in the 316L crosswise section compared to the 17-4PH crosswise section.

Other micrographs of 100x and 500x did not show any notable distinctions apart from one picture of 316L, as shown in Figure 5.11. The austenitic grains in the sample are visible in this section even in the unetched condition. Also, a different phase could be observed between the austenitic grains. However, further analysis must be performed to confirm the findings. In the next section, the etched samples are discussed, which would shed more light on the microstructure of the samples. Lastly, a basic porosity analysis was done on the lengthwise micrographs using a software. The white area in the unetched pictures were attributed to red color and percentage of black pixels were calculated. It was found that, 17-4PH had almost 10% porosity whereas 316L has 3% porosity. However, more testing and data are

needed to draw any conclusions. The pictures used to calculate porosity values are in Appendix A.

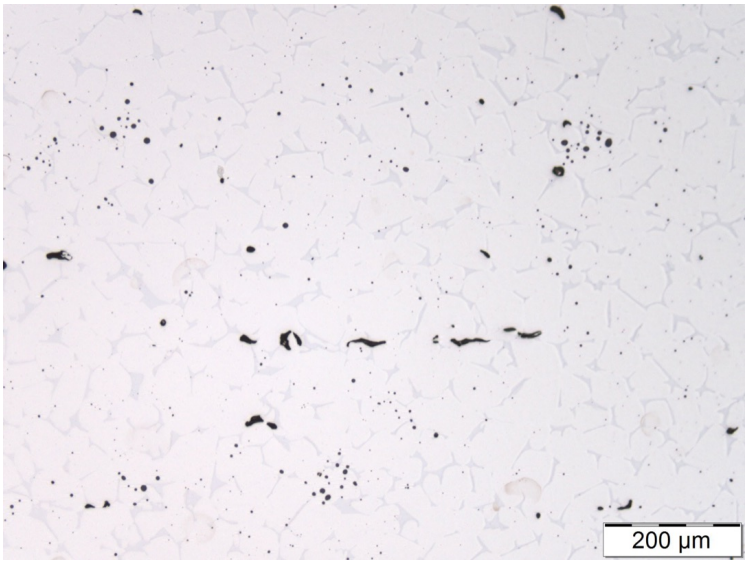

Figure 5.11: 100x zoom micrograph of 316L crosswise unetched sintered sample.

5.9 Metallography: Etched Sintered State

Mostly LOM analysis was performed on all samples. In subsection 5.9.1 where further analysis was required, Energy-dispersive X-ray Spectroscopy (EDX) analysis was also carried out, along with deriving parallels from literature. The investigation was carried out using 100x and 500x zooms to investigate the microstructure of the samples. The lengthwise and crosswise sections showed no peculiar differences. Appendix A contains the micrographs that are not shown in the following subsections. The findings are described in the following subsections.

5.9.1 316L Samples

The state after etching with V2A solution is shown in the Figure 5.12. It is clearly observable that austenitic grains are formed in the sample as visible in Figure 5.12(a). These grain could also be clearly seen in Figure 5.12(b). Soft martensite formation is observed as a needle-shaped microstructure. Further, a different phase is noticed in form of light grey areas between grains (refer Figure 5.12(b))

To analyse the different light grey phase seen in Figure 5.12 between the austenitic grains, further analyses were performed. An analytical measurement system (Oxford

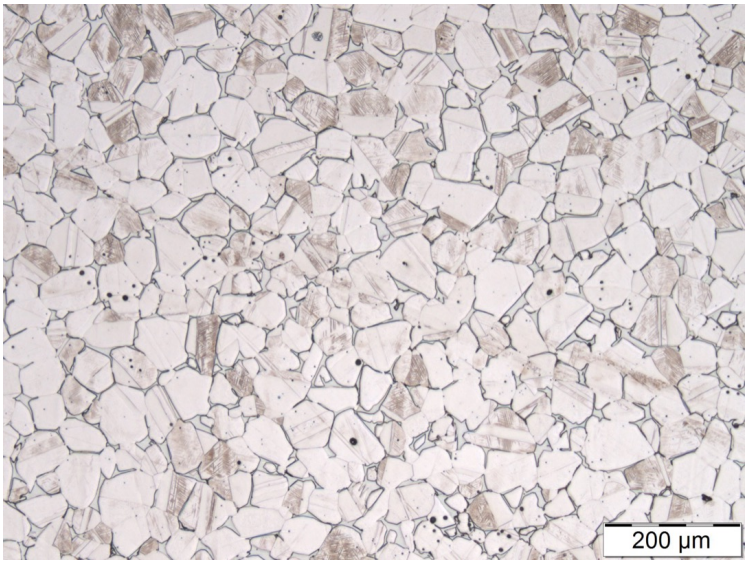

(a) 100x zoom micrograph of etched 316L sample

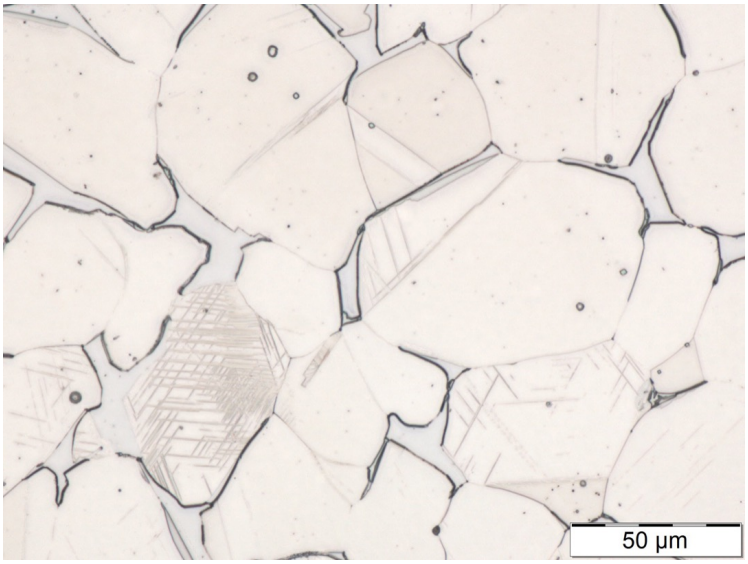

(b) 500x zoom micrograph of etched 316L sample

Figure 5.12: 100x and 500x zoom micrographs of 316L lenghtwise etched samples

Instruments, AzTec) was used for spot analysis. The instrument comes with EDX analysis capabilities, which were used to determine the elemental composition of the light grey areas. These light grey areas could be remnants of binder, which was present in the green state of the sample. Six spots were chosen with different areas for spot analysis, as shown in Figure 5.13. The first four spots represent the light grey phase, and spectrum 5 and 6 represent small areas of the austenitic grains.

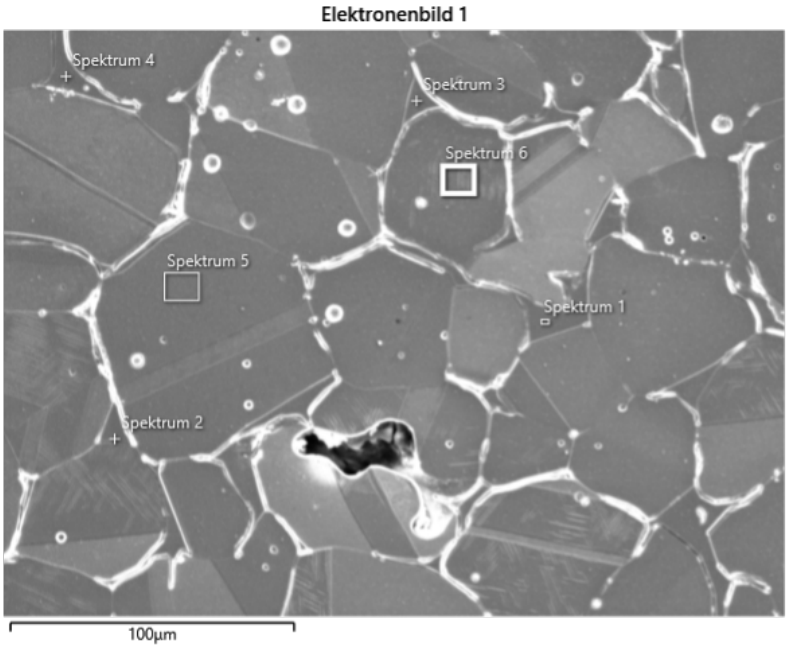

Figure 5.13: EDX analysis positions

The Table 5.8 below shows the EDX results. The carbon content column has been removed from the table as this column is not an accurate representation of the actual carbon content in the analysed spots. This is because the EDX measures the carbon data qualitatively. In addition, carbon concentrations exceeding 3% are typically the result of contamination on the sample surface or the inner surface of the microscope column itself. Lastly, the values measured in the table are in mass percentages.

Table 5.8: EDX analysis results. Values measured in mass percentages.

Spectrum No.	**Si%**	**Cr%**	**Mn%**	**Fe%**	**Ni%**	**Mo%**
1	0.74	23.97	1.25	68.26	5.26	0.52
2	0.74	24.24	1.29	68.30	4.88	0.55
3	0.72	24.57	1.27	68.18	4.74	0.52
4	0.71	23.79	1.32	68.39	5.42	0.38
5	0.56	16.19	1.53	69.89	11.85	0.00
6	0.62	16.68	1.53	69.99	11.18	0.00

After analysing the EDX data, it could be seen that the light grey area mainly consisted of iron element. Thus, this could not be the remnants of the thermoplastic binder. Furthermore, it was observed that the major differences between the light

grey area and the austenitic grain area lie in increased Chromium, decreased nickel, and increased Molybdenum content. Keeping in mind the phase diagram of 316L (refer Figure 5.14) and chromium nickel rich areas found in EDX, it was hypothesized that the light grey area could be the delta ferrite (δ-phase) or sigma phase (σ-phase) [46], [47].

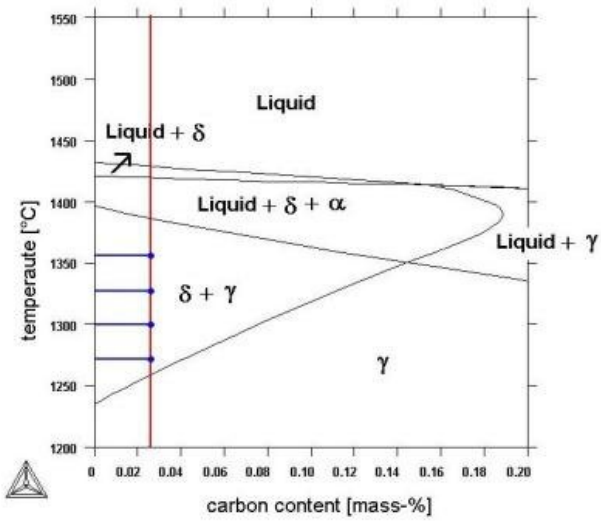

Figure 5.14: Phase diagraom of 316L [46]

To test the above stated hypothesis, the 316L sample was polished and etched again with a sigma phase sensitive etching reagent known as Murakami reagent. It was freshly prepared and heated to 60°C. The sample was kept in the reagent for nearly 5 mins. As shown in Figure 5.15, minimal change was seen. Some small blue contours were seen. These mark the presence of the Sigma phase; however, the majority of the phase between the grains did not get affected by the reagent. Thus some other phase, possibly delta ferrite, might be present and further analysis is needed to determine the phase [43].

Literature was scouted to find similar results, and in a study [48], Binder Jet Process was used to form the 316L specimens. The Binder Jet Process is a 3D printing process where the 3D green part is formed by layering metal powder and binder material alternatively. This forms the green state of the part. After this, powder removal process is performed and then to get a final metal part, the D&S process is performed [49]. Taking into consideration the similarities between binder jetting and MEX 3D printing, the results of the study [48] are used for comparison. The sintering in the binder jet study was done at 1380°C for 2 hours, which is similar

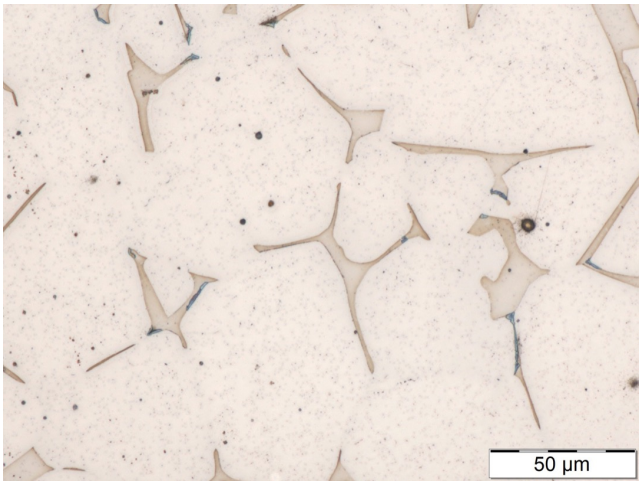

Figure 5.15: 316L Murakami etched sample

to the conditions used to sinter green parts in this study. The results found in the study [48] are shown in the Figure 5.16.

Comparing Figure 5.16 and Figure 5.12(b), extreme similarities could be observed. Thus, it could be concluded that the light grey areas are delta ferrite because of the high ferrite content of the area, negative Murakami reagent test, and comparison with literature. Nevertheless, in order to attain complete certainty, it is essential to conduct further analysis, such as X-Ray Diffraction (XRD).

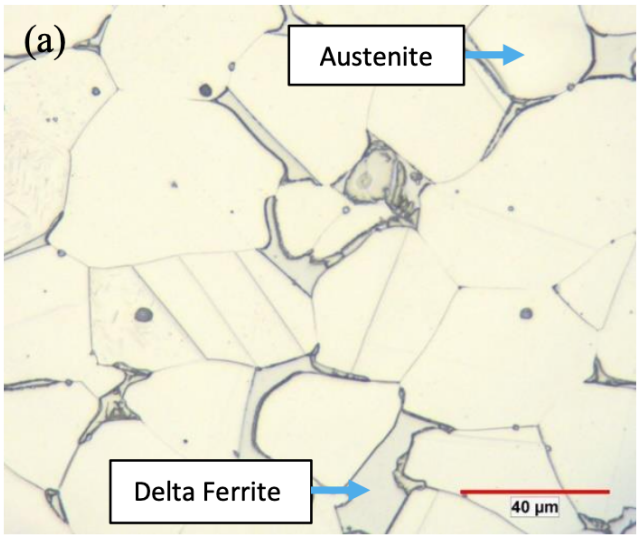

Figure 5.16: 316L microstructure [48]

5.9.2 17-4PH Samples

The state after etching the 17-4PH sample is shown in Figure 5.17. Martensite formation is observed. However, this formation is not the typical pins and needles shape that is usually noticed. It could be observed from Figure 5.17(b) that a different phase other than martensite also seems to be present. As a first step, a simple test with a magnet showed that the sample is magnetic. This could indicate the presence of martensite, ferrite, or both. Further analysis is needed to accurately determine the phases present in the sample.

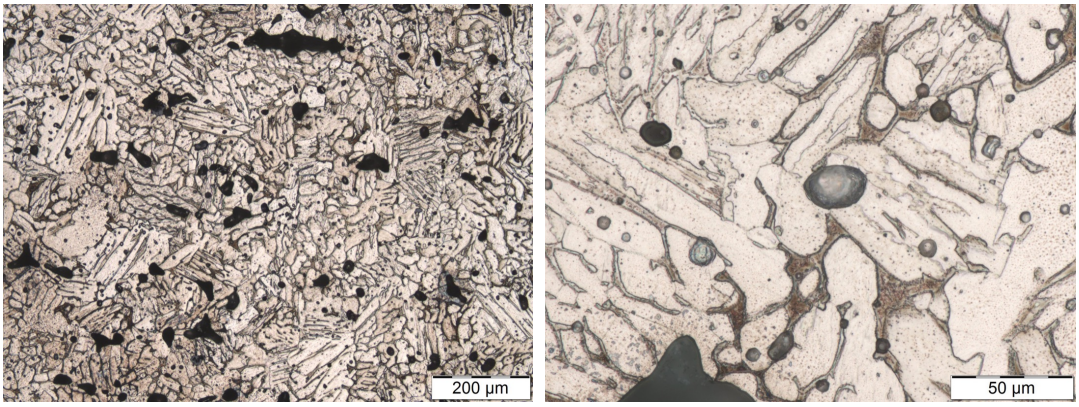

(a) 100x Zoom micrograph (b) 500x Zoom micrograph

Figure 5.17: 100X and 500X Zoom micrographs of 17-4PH lenghwise sintered state of the samples

According to the phase diagram of 17-4PH (refer Figure 5.18), at 1380°C (sintering temperature in this study), delta ferrite (δ) and austenite (γ) both phases are present. The austenite changes to martensite after fast cooling rate. In study [50], similar micrograph results were found where Plasma Assisted Debinding and Sintering (PADS) technology was used to debind and sinter MIM parts. More information on PADS could be found in [51]. Since MIM parts are similar to metal MEX 3D printed parts, and both undergo the D&S process to form final metal parts, the results of the study [50] could be used for comparison and interpolation of results.

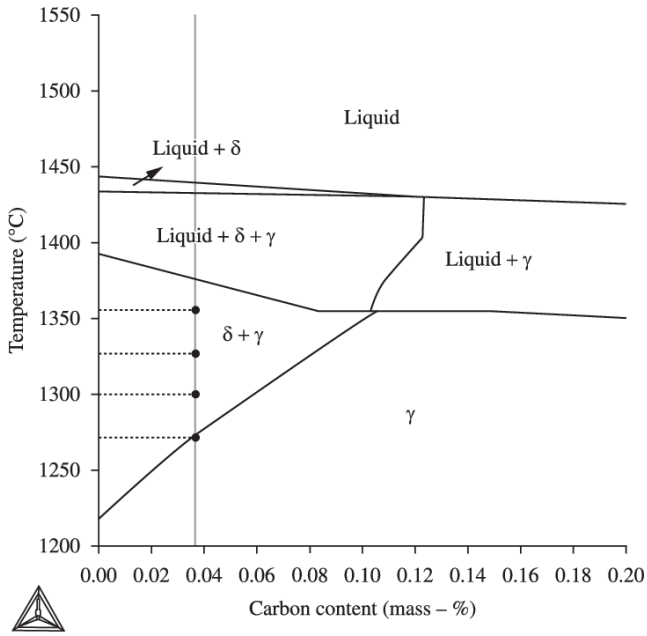

Figure 5.18: 17-4PH phase diagram [46]

The results of the study are shown in Figure 5.19. The study carried out an XRD analysis to determine the microstructural constituents and deduced that martensite and delta ferrite phases are present as visible in Figure 5.19. The Figure 5.17(b) and Figure 5.19 are observed to be very similar. Hence, it could be inferred that Figure 5.17 represent martensite and delta ferrite phases. Also, it could be observed that the martensite phase is predominant. However, further analysis like XRD could be performed to confirm the findings.

Figure 5.19: MIM 17-4PH microstructure sintered in PADS furnance [50].

5.10 Printing Complex Parts

To explore the printing capabilities using metal MEX 3D printer, two complex geometries were printed and one more specimen with both 316L and 17-4PH materials were printed. First, a M10 thread was created in a cube. The goal was to see if precise outcomes could be attained right after D&S process. It was observed that a M10 screw was not completely able to be screwed in the threaded hole. This could have been because of uneven threads. Thus, the hole was tapped once, and after this process, the M10 screw was able to be effortlessly screwed into the threaded hole as shown in Figure 5.20.

Figure 5.20: M10 screw in a 3D printed threaded hole.

Secondly, a miniature version of a turbine blade was printed. The size of the turbine blade in green state could be fitted in 100x100x100 mm cube. For the first try, the turbine blade cracked near the the sharp unsupported edge of the blade as shown in the Figure 5.21.

Figure 5.21: Cracked turbine blade after D&S process.

It was hypothesized that the turbine blade cracked due to its thinness. This blade needed to be properly supported, and hence, the orientation of the blade was changed as seen in the Figure 5.22(a). This part was sent for the D&S process, and it successfully went through the D&S process. The final metal blade could be seen in Figure 5.22(b). This shows the importance of orientation when printing with metal MEX technology.

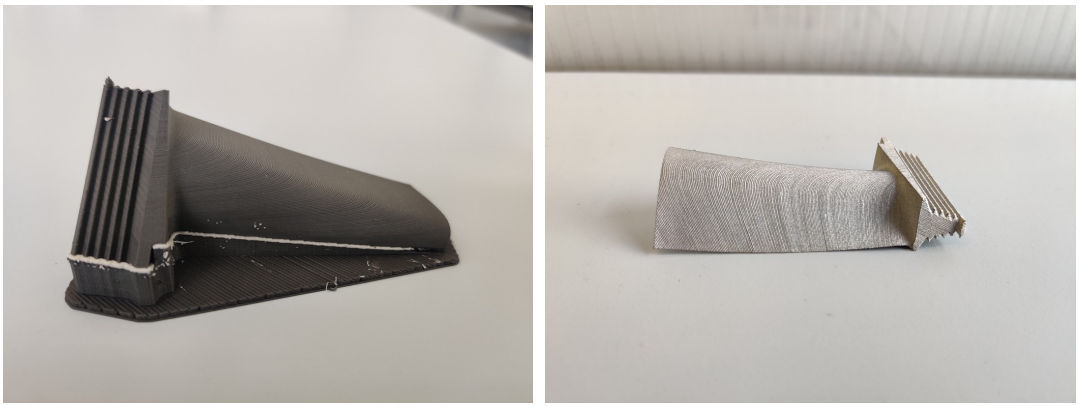

(a) Green state of the miniature turbine blade with changed orientation.

(b) Sintered state of the miniature turbine blade

Figure 5.22: Miniature model of turbine blade printed using Metal MEX technology

Lastly, one more sample was printed. This sample had simple geometry however, it contained two separate material. A layered sample, similar to the one used in Metallographic analysis, was sent for D&S process to explore the possibility of printing and sintering separate materials together. The sample was received without any cracks as seen in the Figure 5.23. Further metallographic analysis could be performed on a cross section of the sample to view the microstructure near the interface between 316L and 17-4PH.

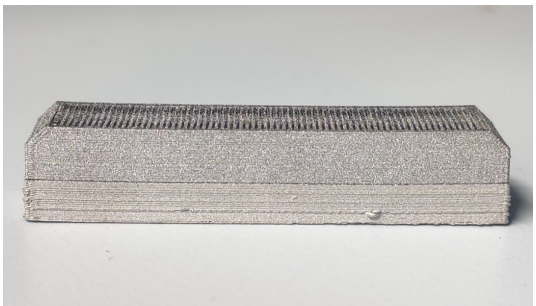

Figure 5.23: Sintered layered sample consisting of two separate layers: 316L and 17-4PH

Chapter 6

Conclusion

One of the main aims of this thesis was to build up knowledge about metal MEX 3D printing at the Rhine-Waal University of Applied Sciences. There has been a lot of progress made in this direction, and many different facets of the technology have been investigated and, more importantly, experimentally tested. This study extends the current state of knowledge about the material properties of metal MEX 3D printed parts. Moreover, the effect of surface roughness on the strength of materials was also studied. In the literature, this effect has been sparsely investigated.

In general, it was seen that the tensile strength of the materials remained unchanged between unpolished and polished specimens for both materials. This contradicted the initial hypothesis made in this study. Furthermore, the polished specimens showed slightly better yield strength than the unpolished specimens.

The strength of the materials found was comparatively low compared to the released data by the manufacturer of the filament, BASF. This could be because BASF used milled specimens, whereas in this thesis, as-printed specimens with one side milled were used. Further, the fabrication of the on-edge tensile bar of form E5x16x55, according to DIN 50125, was not successful, and more iterations are needed to produce an uncracked specimen. Nonetheless, a smaller version of the on-edge tensile bar (form E4x10x35 according to DIN 50125) was successfully fabricated and tested. Surprisingly, it showed better strength properties than flat tensile bars. However, more testing is needed to draw any final conclusions.

The evolution of surface roughness from the green state to the sintered state was also studied. The results from this study suggest that there is a clear relationship between surface roughness and change in state (from green to sintered). It was seen that the surface roughness drastically increased after the D&S process. On the other

hand, no clear evidence was found to suggest that surface roughness increases more in unpolished samples than in polished samples after the D&S process.

Furthermore, the density values of green and sintered samples were also determined. The theoretical density of green parts was found to be 4878 and 4351 kg/m^3 for 316L and 17-4PH, respectively. In the sintered state, the theoretical densities were found to be 79521 and 7260 kg/m^3 for 316L and 17-4PH, respectively. In all, 17-4PH showed better strength properties even though it was less dense than 316L, whereas 316L was drastically more ductile than 17-4PH.

Shrinkage was also determined and found to be similar to values released by the manufacturer in the XY plane. However, the shrinkage in the printing direction (Z) was 3% less than the data released by BASF. This was attributed to slightly faulty thickness measurements due to the presence of sharp edges (similar to a metal burr) on the contour of the samples. Between 316L and 17-4PH, shrinkage was slightly higher in 17-4PH specimens. However, generally speaking, both have similar shrinkage values as specified by the manufacturer.

The goal of primary metallographic analysis of 316L and 17-4PH samples was also met. 316L was seen to be austenitic, with the presence of delta ferrite in between grains. For 17-4PH, it was determined that it was martensitic with the presence of delta ferrite. A high level of porosity was found in the samples. With primary porosity analysis using software, it was determined that 17-4PH has almost 10% porosity and 316L has 3% porosity.

Lastly, an extra experiment was performed. The aim of this was to check if a layered sample (bottom layer of 316L and top layer of 17-4PH) could be prepared. It was seen that such a sample could be successfully created and sintered. This opens door to combinations of the materials, 316L and 17-4PH, so that advantages of individual material properties could be taken, such as strength and anti-corrosion properties.

6.1 Potential of Metal Material Extrusion 3D Printing

In this section, the author's view and experience with the technology have been briefly expressed. It is believed by the author that Metal MEX technology has great potential for fabricating small parts. In the maintenance market, manufacturers of machines sometimes stop producing machine spare parts. However, a large number of customers of the machine would still like to replace a broken or malfunctioning part that is no longer produced by the manufacturer. This is an area where the customers could themselves cheaply produce the desired parts according to their specifications, or alternatively, the manufacturer could print the parts and deliver them to the customer. This way, the manufacturer also does not have to maintain

any spare parts inventory. Another potential field where there is a huge possibility of application is the mould market. Some times a mould with high tolerances and finish is not needed. This is an area that presents an opportunity for the use of metal MEX technology to drag the cost of making moulds down. Even making mould with low tolerances could be an expensive process. At the same time, it has to kept in mind that this technology comes with some difficulties such as porosity and uneven shrinkages.

However, this technology is still in its infancy, and inconsistencies with the performance of the technology need to be tackled using systematic investigation methods. Nonetheless, it is believed that this technology shows potential and should be researched further at Rhein-Waal University of Applied Sciences.

Chapter 7

Future Work

This thesis and research have opened up new research questions. These questions could be used as the basis for future theses and research topics. The following topics could be investigated further.

1. More iterations for producing on-edge tensile bars could be performed, and finally, the effect of build orientation on the strength of the material could be analyzed.
2. Fatigue and hardness testing could be performed on the samples. Papers [5] could be used as a starting point.
3. The influence of heat treatment could be studied on 17-4PH as it is seen from literature that it could have considerably higher tensile strength properties after heat treatment [16], [44].
4. In this thesis, a threaded hole was printed successfully. This direction could be further explored, and the strength of bolted joints could be determined.
5. More metallographic analysis could be performed on the materials, such as XDR analysis, to confirm the microstructure of the materials. Further, the grain size could be determined as per DIN EN ISO 643.
6. In this thesis, it was shown that 316L and 17-4PH could be successfully combined. Also, after contacting BASF, it has been found out that printing tensile bars with different outside and inside materials is possible. Thus, the combination of 316L and 17-4PH materials could be explored. Tensile testing could be performed and compared to each material's properties.
7. Die/Mould making of small parts could be explored by making small mould for injection moulded parts.

8. Simulation analysis could be explored to predict cracks in the part during debinding or sintering phases [52]. Live Sinter software could also be explored for sintering simulation.

9. The printed green parts could be tried to be sintered inhouse for more control on the heating and cooling parameters.

Bibliography

[1] L. Gardner, P. Kyvelou, G. Herbert, and C. Buchanan, "Testing and initial verification of the world's first metal 3D printed bridge," *Journal of Constructional Steel Research*, vol. 172, p. 106 233, Sep. 2020.

[2] S. Roshchupkin, A. Kolesov, A. Tarakhovskiy, and I. Tishchenko, "A brief review of main ideas of metal fused filament fabrication," *Materials Today: Proceedings*, vol. 38, pp. 2063–2067, Sep. 2021. [Online]. Available: `https://explore.openaire.eu/search/publication?pid=10.1016%2Fj.matpr.2020.10.142`.

[3] *Different types of 3D metal printing.* [Online]. Available: `https://markforged.com/de/resources/learn/design-for-additive-manufacturing-metals/metal-additive-manufacturing-introduction/types-of-3d-printing-metal`.

[4] ISO/ASTM 52900, "Additive manufacturing-General principles-Fundamentals and vocabulary Fabrication, International Standard ISO/ASTM 52900:2021(E)," Tech. Rep., 2023. [Online]. Available: `www.astm.org`.

[5] S. Kedziora, T. Decker, E. Museyibov, *et al.*, "Strength Properties of 316L and 17-4 PH Stainless Steel Produced with Additive Manufacturing," *Materials*, vol. 15, no. 18, Sep. 2022. [Online]. Available: `https://www.researchgate.net/publication/363407372_Strength_Properties_of_316L_and_17-4_PH_Stainless_Steel_Produced_with_Additive_Manufacturing`.

[6] H. Ramazani and A. Kami, "Metal FDM, a new extrusion-based additive manufacturing technology for manufacturing of metallic parts: a review," *Progress in Additive Manufacturing*, vol. 7, no. 4, pp. 609–626, Aug. 2022. [Online]. Available: `https://www.researchgate.net/publication/358037836_Metal_FDM_a_new_extrusion-based_additive_manufacturing_technology_for_manufacturing_of_metallic_parts_a_review`.

[7] C. Tosto, J. Tirillò, F. Sarasini, and G. Cicala, "Hybrid metal/polymer filaments for fused filament fabrication (FFF) to print metal parts," *Applied Sciences (Switzerland)*, vol. 11, no. 4, p. 1, Feb. 2021.

[8] T. Kurose, Y. Abe, M. V. A. Santos, *et al.*, "Influence of the Layer Directions on the Properties of 316L Stainless Steel Parts Fabricated through Fused Deposition of Metals," *Materials*, vol. 13, no. 11, p. 2493, May 2020. [Online]. Available: https://www.mdpi.com/1996-1944/13/11/2493.

[9] C. Tosto, J. Tirillò, F. Sarasini, C. Sergi, and G. Cicala, "Fused Deposition Modeling Parameter Optimization for Cost-Effective Metal Part Printing," *Polymers 2022, Vol. 14, Page 3264*, vol. 14, no. 16, p. 3264, Aug. 2022. [Online]. Available: https://www.mdpi.com/2073-4360/14/16/3264.

[10] J. Gonzalez-Gutierrez, F. Arbeiter, T. Schlauf, C. Kukla, and C. Holzer, "Tensile properties of sintered 17-4PH stainless steel fabricated by material extrusion additive manufacturing," *Materials Letters*, vol. 248, pp. 165–168, Aug. 2019. [Online]. Available: https://www.researchgate.net/publication/332343374_Tensile_properties_of_sintered_17-4PH_stainless_steel_fabricated_by_material_extrusion_additive_manufacturing.

[11] D. Godec, S. Cano, C. Holzer, and J. Gonzalez-Gutierrez, "Optimization of the 3D Printing Parameters for Tensile Properties of Specimens Produced by Fused Filament Fabrication of 17-4PH Stainless Steel," *Materials 2020, Vol. 13, Page 774*, vol. 13, no. 3, p. 774, Feb. 2020. [Online]. Available: https://www.mdpi.com/1996-1944/13/3/774.

[12] I. Chang Dr and Y. Zhao, "Advances in powder metallurgy: Properties, processing and applications," *Advances in Powder Metallurgy: Properties, Processing and Applications*, pp. 1–604, 2013. [Online]. Available: https://www.researchgate.net/publication/316698054_Advances_in_powder_metallurgy_Properties_processing_and_applications.

[13] C. Suwanpreecha and A. Manonukul, "A Review on Material Extrusion Additive Manufacturing of Metal and How It Compares with Metal Injection Moulding," *Metals 2022, Vol. 12, Page 429*, vol. 12, no. 3, p. 429, Feb. 2022. [Online]. Available: https://www.mdpi.com/2075-4701/12/3/429.

[14] "BASF 3D Printing Solutions Technical Data Sheet Ultrafuse® 316L," Tech. Rep. [Online]. Available: https://move.forward-am.com/hubfs/AES%20Documentation/Metal%20Filaments/316L/TDS/Ultrafuse_316L_TDS_EN_v1.1.pdf.

[15] "BASF 3D Printing Solutions, Technical Data Sheet, Ultrafuse® 17-4 PH," Tech. Rep. [Online]. Available: https://move.forward-am.com/hubfs/AES%20Documentation/Metal%20Filaments/17-4%20PH/TDS/Ultrafuse_17-4PH_TDS_EN_v1.1.pdf.

[16] A. Pellegrini, F. Lavecchia, M. G. Guerra, and L. M. Galantucci, "Influence of aging treatments on 17–4 PH stainless steel parts realized using material extrusion additive manufacturing technologies," *International Journal of Advanced Manufacturing Technology*, vol. 126, no. 1, pp. 163–178, May 2023.

[Online]. Available: https://link.springer.com/article/10.1007/s00170-023-11136-3.

[17] "Ultrafuse ® Metal Filaments User Guidelines for 3D Printing Metal Parts," Tech. Rep. [Online]. Available: https://forward-am.com/wp-content/uploads/2021/04/UserGuidelines_2021_03_29.pdf.

[18] "Markforged Design Guide for 3D Printing with Metals," Tech. Rep. [Online]. Available: https://newforge.com.au/wp-content/uploads/2022/04/New_Forge_Metal_Design_Guide.pdf.

[19] "BMD Design Guide Studio System™," Tech. Rep. [Online]. Available: https://www.desktopmetal.com/uploads/Desktop-Metal-BMD-Design-Guide.pdf.

[20] "Ultrafuse® Support Layer Technical Data Sheet," Tech. Rep. [Online]. Available: www.forward-am.com..

[21] Basf, "Ultraform (POM) – Product Brochure," Tech. Rep. [Online]. Available: www.plasticsportal.eu/ultraform.

[22] "Troubleshooting Guide Green Part and Shipping," Tech. Rep.

[23] "Fused Deposition Modeling Based 3D Printing," Materials Forming, Machining and Tribology, H. K. Dave and J. P. Davim, Eds., 2021. [Online]. Available: https://link.springer.com/10.1007/978-3-030-68024-4.

[24] "BASF Process Instructions Ultrafuse316L,"

[25] "Debinding Simulation Guidelines for 3D Printed Parts using Ultrafuse ® 316L," Tech. Rep. [Online]. Available: www.forward-am.com.

[26] A. Pellegrini, M. E. Palmieri, and M. G. Guerra, "Evaluation of anisotropic mechanical behaviour of 316L parts realized by metal fused filament fabrication using digital image correlation," *International Journal of Advanced Manufacturing Technology*, vol. 120, no. 11-12, pp. 7951–7965, Jun. 2022. [Online]. Available: https://link.springer.com/article/10.1007/s00170-022-09303-z.

[27] "DIN 50125 Testing of metallic materials -Tensile test pieces," Tech. Rep., 2009. [Online]. Available: www.din.de.

[28] "Metallic materials-Tensile testing-Part 1: Method of test at room temperature," Tech. Rep., 2019. [Online]. Available: www.iso.org.

[29] "Geometrical Product Specifications (GPS) -Surface texture: Profile method - Terms, definitions and surface texture parameters. ISO 4287-2:1997," Tech. Rep., 1997. [Online]. Available: www.beuth.deGesamtumfang27Seiten07/14/202317:22:29HochschulbibliothekszentrumdesLandesNordrhein-Westfalen.

[30] M. Harcarik and R. Jankovych, "Relationship between values of profile and areal surface texture parameters," *MM Science Journal*, vol. 2016, no. DECEMBER, pp. 1659–1662, Dec. 2016. [Online]. Available: https://www.mmscience.eu/journal/issues/december-2016/articles/relationship-between-values-of-profile-and-areal-surface-texture-parameters.

[31] "Geometrical product specifications (GPS) - Surface texture: Areal - Part 2: Terms, definitions and surface texture parameters. ISO 25178-2:2012.," Tech. Rep., 2012. [Online]. Available: www.din.de.

[32] Olympus, *Surface Roughness Measurement—Parameters*. [Online]. Available: https://www.olympus-ims.com/en/metrology/surface-roughness-measurement-portal/parameters/#!cms[focus]=024.

[33] R. Leach, *Characterisation of areal surface texture*. Springer-Verlag Berlin Heidelberg, Jun. 2013, vol. 9783642364587, pp. 1–353.

[34] Keyence, *Introduction to Surface Roughness Measurement*. [Online]. Available: https://sernia.ru/upload/pdf_files/Introduction%20to%20surface%20roughness%20measurement.pdf.

[35] Ultimaker, "Ultimaker S5 Product Datasheet," Tech. Rep. [Online]. Available: https://www.shop3d.gr/wp-content/uploads/2022/01/Ultimaker-S5-Pro-bundle.pdf.

[36] *UltiMaker S5 + Air Manager*. [Online]. Available: https://www.crea3d.com/en/ultimaker-3d-printers/1148-promo-ultimaker-s5-air-manager.html.

[37] Ultimaker, "Ultimaker S5 Air Manager product datasheet," Tech. Rep. [Online]. Available: https://www.shop3d.gr/wp-content/uploads/2022/01/Ultimaker-S5-Pro-bundle.pdf.

[38] "Ultimaker Metal Expansion Kit Product Sheet-en," Tech. Rep. [Online]. Available: https://sourcegraphics.com/wp-content/uploads/2022/08/ultimaker-metal-expansion-kit-product-sheet-en-sg.pdf.

[39] "Ultimaker Print Core DD Datasheet," [Online]. Available: https://docs.rs-online.com/f01e/A700000009233992.pdf.

[40] "Shimadzu AG-X-V2 Series Datasheet," Tech. Rep. [Online]. Available: https://www.shimadzu.com/an/sites/shimadzu.com.an/files/pim/pim_document_file/brochures/17011/c224-e122.pdf.

[41] J. Ramirez, "Surface Roughness Statistical Analysis Using 3D Profilometry," 2012.

[42] J. Antoy, "Design of Experiments for Engineers and Scientists: Second Edition," *Design of Experiments for Engineers and Scientists: Second Edition*, pp. 1–672, 2014.

[43] G. Petzow, *Metallographic Etching, 2nd Edition Techiniques for Metallography, Ceramography, Plastography*, 1999. [Online]. Available: https://www.google.de/books/edition/Metallographic_Etching_2nd_Edition/8N6b5B7bEVsC?hl=en&gbpv=1&dq=bibliogroup:%22Techniques+for+metallography,+ceramography,+plastography%22&printsec=frontcover.

[44] Y. Abe, T. Kurose, M. V. Santos, *et al.*, "Effect of Layer Directions on Internal Structures and Tensile Properties of 17-4PH Stainless Steel Parts Fabricated by Fused Deposition of Metals," *Materials 2021, Vol. 14, Page 243*, vol. 14, no. 2, p. 243, Jan. 2021. [Online]. Available: https://www.mdpi.com/1996-1944/14/2/243.

[45] "BASF 3D Printing Solutions, Technical Data Sheet, Ultrafuse® PLA," Tech. Rep. [Online]. Available: www.basf-3dps.com.

[46] *Thermodynamic simulation of 316L and 17-4PH stainless steels using different process conditions for two components metal injection moulding (2C-MIM).* [Online]. Available: https://www.researchgate.net/publication/287029518_Thermodynamic_simulation_of_316L_and_17-4PH_stainless_steels_using_different_process_conditions_for_two_components_metal_injection_moulding_2C-MIM.

[47] C.-C. Hsieh and W. Wu, "Overview of Intermetallic Sigma (σ) Phase Precipitation in Stainless Steels," vol. 2012, p. 16, 2012. DOI: 10.5402/2012/732471.

[48] K. Horvay, C. Schade, and T. Murphy, "Development of 316L, 2507 Duplex and Nickel-Free Stainless Steel for the Binder Jet Process,"

[49] M. Ziaee and N. B. Crane, "Binder Jetting: A Review of Process, Materials, and Methods," *Additive Manufacturing*, vol. 28, pp. 781–80, 2019. [Online]. Available: https://scholarsarchive.byu.edu/facpub.

[50] R. Schroeder, G. Hammes, C. Binder, and A. N. Klein, "Plasma Debinding and Sintering of Metal Injection Moulded 17-4PH stainless steel," *Materials Research*, vol. 14, no. 4, pp. 564–568, Oct. 2011.

[51] R. Machado, W. Ristow, P. Alba, A. N. Klein, P. A. Wendhausen, and D. Fusão, "Plasma Assisted Debinding and Sintering (PADS) – Metal Injection Molding Application," *Materials Science Forum*, vol. 530-531, pp. 224–229, Nov. 2006.

[52] T. Rosnitschek, J. Glamsch, C. Lange, B. Alber-Laukant, and F. Rieg, "An Automated Open-Source Approach for Debinding Simulation in Metal Extrusion Additive Manufacturing," *Designs 2021, Vol. 5, Page 2*, vol. 5, no. 1, p. 2, Jan. 2021. [Online]. Available: https://www.mdpi.com/2411-9660/5/1/2.

Appendix A

Appendix

I Figures

This section contains supplementary figures that could help the reader get a deeper understanding. The figures are not described, but nonetheless, they can offer more insight into the metal MEX 3D printing technology.

Figure A.1: Rough surface of the specimen that was milled afterwards.

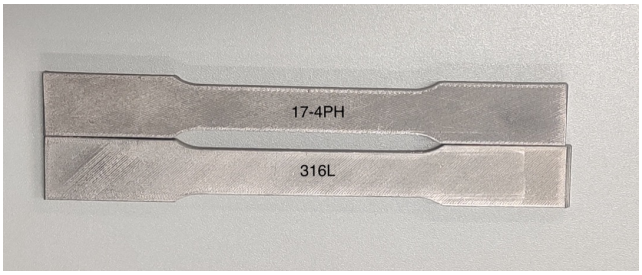

Figure A.2: Different shrinkages in the length of 17-4PH and 316L specimens.

I.1 Surface Roughness

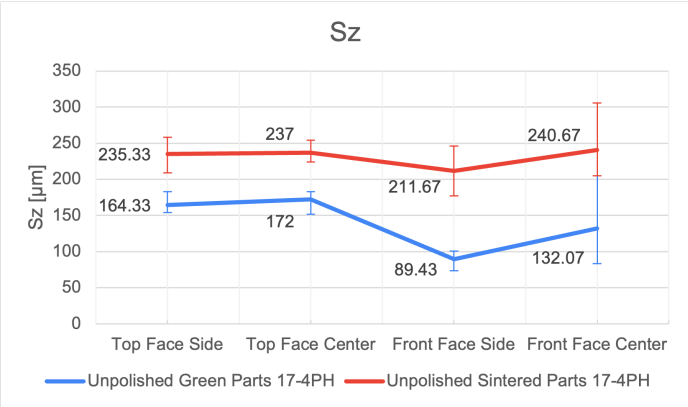

(a) Sz of 17-4PH specimens

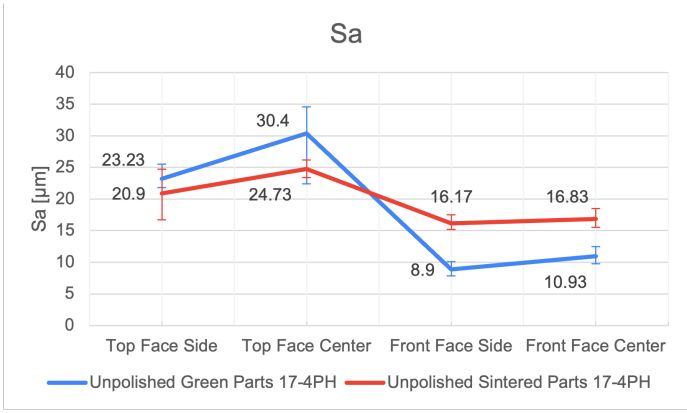

(b) Sa of 17-4PH specimens

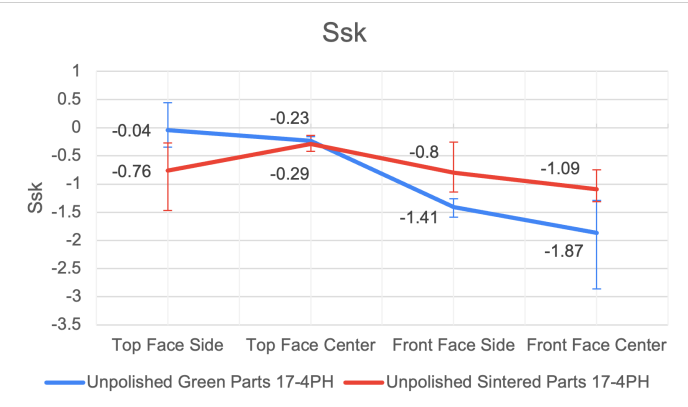

(c) Skewness of 17-4PH specimens

Figure A.3: Plot of surface rouhness parameters of 17-4PH unpolished specimens.

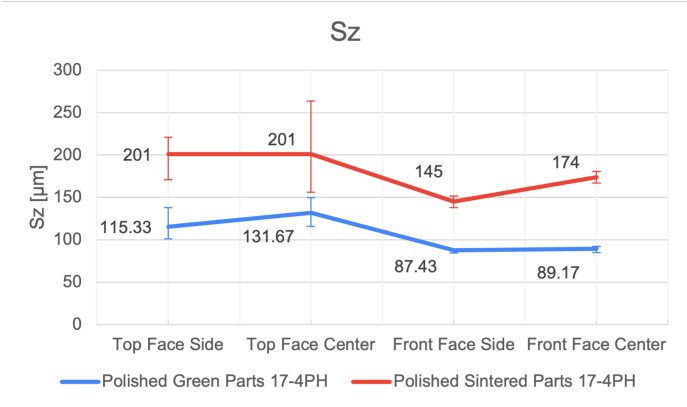

(a) Sz of 17-4PH specimens.

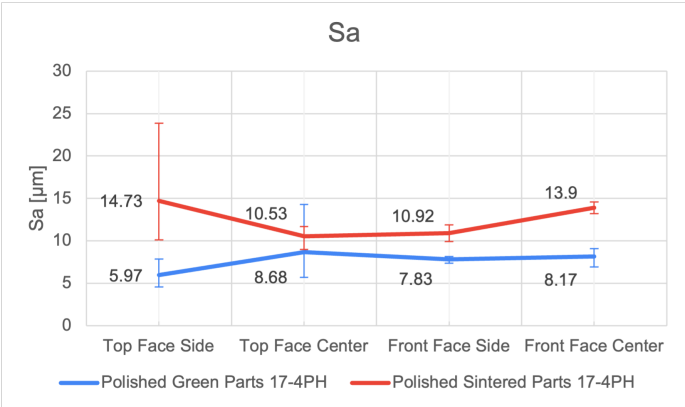

(b) Sa of 17-4PH specimens.

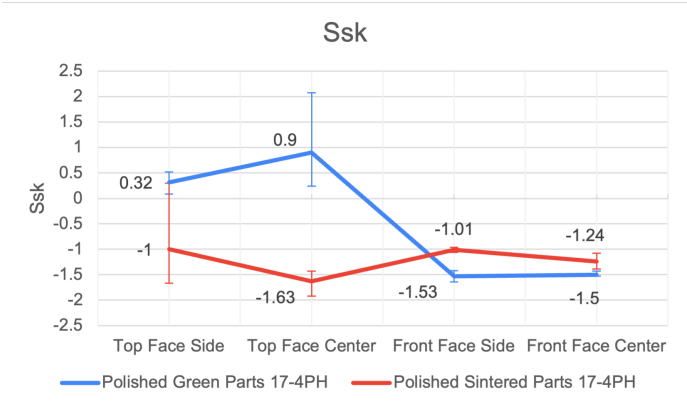

(c) Skewness of 17-4PH specimens.

Figure A.4: Plots of surface rouhness parameters of 17-4PH polished specimens.

I.2 Metallography

I.2.1 Green Samples

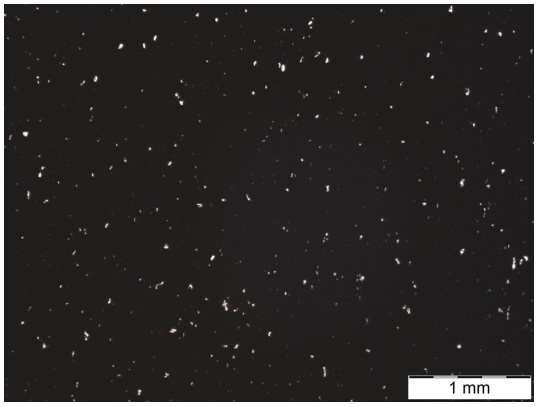

(a) Micrograph of 17-4PH green sample.

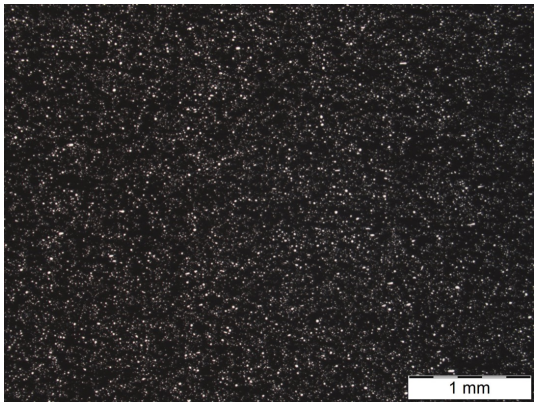

(b) Micrograph of 316L green sample.

Figure A.5: 25x zoom micrographs of green lengthwise samples.

I.2.2 Porosity Measurements

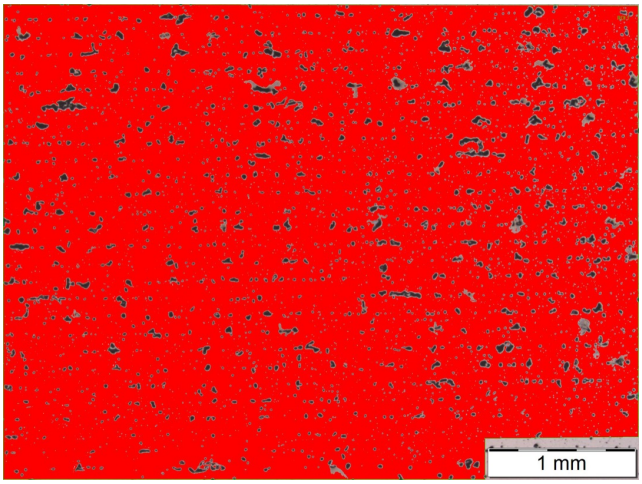

(a) 10% porosity measured in 17-4PH unetched sintered sample.

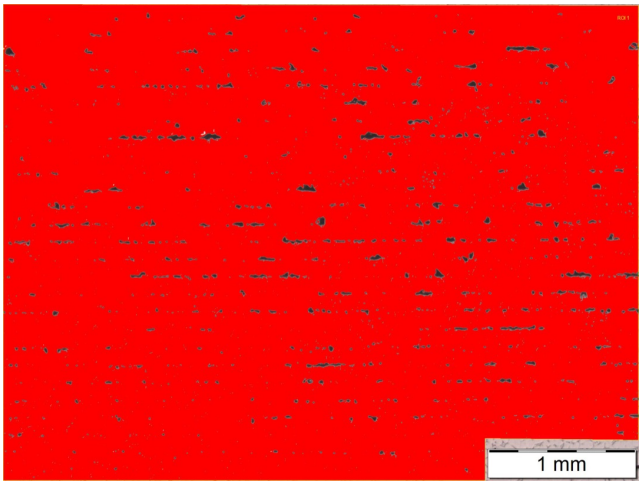

(b) 3% porosity measured in 316L unetched sintered sample.

Figure A.6: Porosity measurements in unetched sintered samples.

I.2.3 Sintered Etched Samples

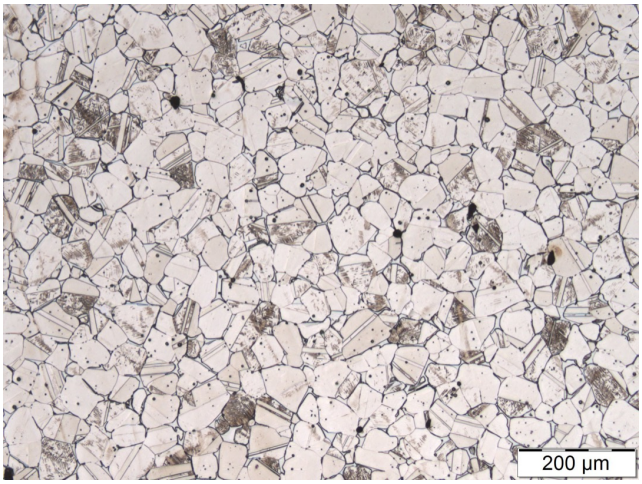

(a) 100x zoom micrograph of etched 316L sample.

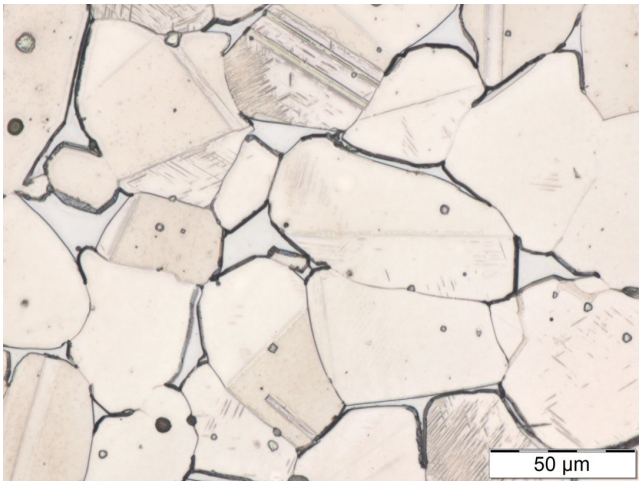

(b) 500x zoom micrograph of etched 316L sample.

Figure A.7: Micrographs of 316L sintered crosswise etched samples. Etched with V2A solution.

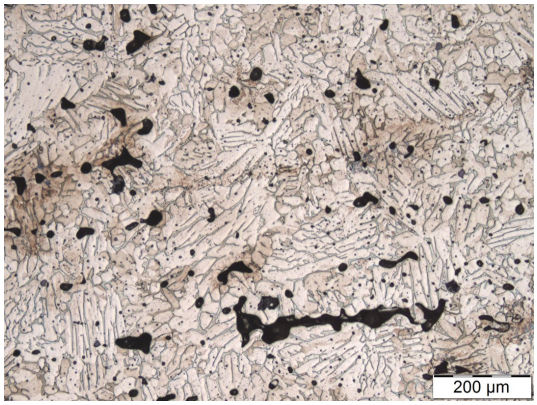

(a) 100x zoom micrograph of etched 17-4PH sample.

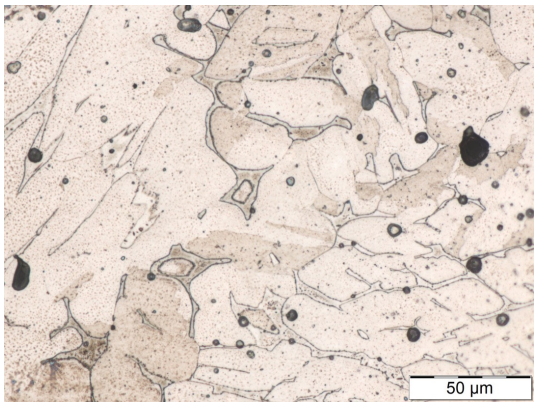

(b) 500x zoom micrograph of etched 17-4PH sample.

Figure A.8: Micrographs of 17-4PH sintered crosswise etched samples. Etched with V2A solution.

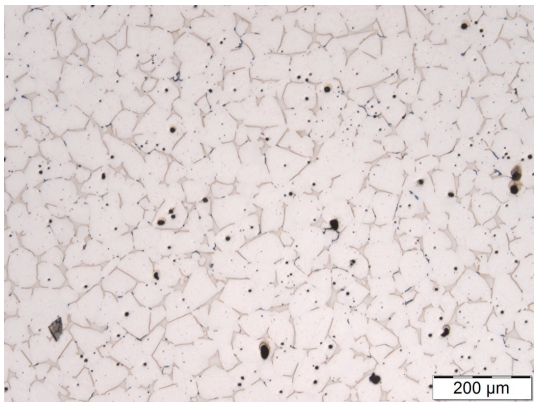

Figure A.9: 100x zoom micrographs of 316L sintered crosswise etched samples. Etched with Murakami reagent.

II Printing Parameters

Most of the printing was done using default parameters given by BASF and recommendations in [22]. Some important printing parameters are given in the table below:

Table A.1: Some important printing parameters used in Ultimaker S5 printer.

Parameter	**Used value**
Retraction distance	5 mm
Retraction speed	45 mm/s
Layer height	0.15 mm
Infill Density	105%
Infill Overlap Percentage	30
Nozzle temperature	240° C
Bed temperature	100° C
Print speed	30 mm/s
X and Y oversizing factors	120%
Z oversizing factor	126%